THE GEOLOGICAL SOCIETY OF AMERICA®

Late Cretaceous magmatism in the NW Lhasa Terrane, southern Tibet: Implications for crustal thickening and initial surface uplift

Ming Lei[1,2], Jian-Lin Chen[1,3,†], Ji-Feng Xu[1,3], Yun-Chuan Zeng[1,2], and Qiu-Wei Xiong[1,2]

[1]*State Key Laboratory of Isotope Geochemistry, Guangzhou Institute of Geochemistry, Chinese Academy of Sciences, Guangzhou 510640, China*

[2]*University of Chinese Academy of Sciences, Beijing 100049, China*

[3]*CAS Center for Excellence in Tibetan Plateau Earth Sciences, China*

ABSTRACT

Crustal thickening and uplift of southern Tibet have been widely associated with India-Asia continental collision during the Cenozoic. However, recent studies indicated that the crust of the northwestern (NW) Lhasa Terrane was thickened during the late Mesozoic. Here we report geochronological and geochemical data for the Gaerqiong diorite porphyries (GPs) and Xiongma plutons (XPs) in the NW Lhasa terrane, southern Tibet. Zircon U-Pb dating suggests that these intrusive rocks were generated at ca. 85 and ca. 88 Ma, respectively. The GPs are characterized by high MgO, Cr, and Ni contents, and they have adakitic affinities. These geochemical features, combined with their depleted $\varepsilon Nd_{(t)}$ (+1.7 to +2.0), $^{87}Sr/^{86}Sr_{(i)}$ (0.705103–0.705259), and zircon $\varepsilon Hf_{(t)}$ (+5.2 to +10.2) isotopic compositions, indicate that the GPs were produced by partial melting of the delaminated juvenile continental crust. In contrast, the XPs are composed of host granites and mafic microgranular enclaves (MMEs). The MMEs have low SiO_2 and high MgO contents, and low $\varepsilon Hf_{(t)}$ (–14.0 to –5.8) values, indicating that their parental magmas were derived from an enriched mantle. The host granites have high SiO_2 and low MgO contents, and variable $\varepsilon Nd_{(t)}$ (–7.4 to –6.3) and zircon $\varepsilon Hf_{(t)}$ (–11 to –4.1) values. These observations, combined with the presence of MMEs in the Xiongma granites, suggest that the host granites were the result of mixing of crust- and mantle-derived magmas. Detailed study of these two plutons, combined with the previous researches, suggests that Late Cretaceous (ca. 90 Ma) magmatism in the NW Lhasa Terrane occurred in a post-collisional extensional setting related to delamination of the regionally thickened lithosphere after collision of the Lhasa-Qiangtang Terranes. We propose that the crust of the NW Lhasa Terrane reached a maximum thickness (average of >50 km) before the Late Cretaceous (ca. 90 Ma). This crustal thickening was caused by underplating of mafic magmas during slab roll-back and break-off of the southward-subducting Bangong-Nujiang oceanic lithosphere and subsequent tectonic thrusting during Qiangtang-Lhasa Terrane collision, respectively. Given that crustal thickening generally results in elevated terrain, the regional uplift (driven by isostasy due to crustal thickening) probably commenced before the Late Cretaceous (ca. 90 Ma).

INTRODUCTION

The Tibetan Plateau has the highest average altitude and thickest crust on Earth (Yin and Harrison, 2000). However, the timing and mechanism of uplift are still debated (Fielding, 1996; Wang et al., 2008). The plateau uplift and crustal thickening of Tibet were previously associated with collision between the Eurasian and Indian plates during the Cenozoic (e.g., Yin and Harrison, 2000). Several geodynamic models have been proposed to explain the Cenozoic uplift of the Tibetan Plateau, including: (1) removal of the lower lithosphere by convective mantle (Turner et al., 1996; Chung et al., 1998); (2) continental subduction (Tapponnier et al., 2001; Ding et al., 2003); and (3) slab break-off (Davies and von Blanckenburg, 1995; Mahéo et al., 2002). In contrast, tectonic and sedimentary studies have documented that the crust of the northwestern (NW) Lhasa Terrane was significantly thickened and uplifted during the Cretaceous (Murphy et al., 1997; Kapp et al., 2007; Volkmer et al., 2007; Sun et al., 2015a; Wang et al., 2017). However, Zhang et al. (2012) suggested that the NW Lhasa Terrane still remained at sea level until the earliest Late Cretaceous (early Cenomanian). Thus, reconstruction of the crustal thickening and uplift history of the NW Lhasa Terrane since the Cretaceous is critical for understanding the timing of the early topographic growth of the Tibetan Plateau.

During the Mesozoic, the NW Lhasa Terrane experienced southward subduction of the Bangong-Nujiang oceanic slab along its northern boundary, and northward subduction of the Neo-tethyan oceanic slab along its southern boundary (Pan et al., 2006; Zhu et al., 2013; Wang et al., 2016a). Previous studies showed that Cretaceous intermediate-silicic rocks have a widespread distribution in the NW Lhasa Terrane (Zhu et al., 2009, 2011). The La/Yb and Sr/Y values of continental intermediate-silicic rocks are often positively correlated with crustal thickness (Chapman et al., 2015; Profeta et al., 2015). Consequently, these indices for the Cretaceous intermediate-silicic rocks may provide a better constraint on the commencement of Tibetan plateau uplift. However, it is uncertain as to whether the generation of these Cretaceous intermediate-silicic rocks in the NW Lhasa Terrane was controlled by either the evolution of the Neo-tethyan (Indus–Yarlung Zangbo) oceanic lithosphere or Bangong-Nujiang oceanic lithosphere (Zhao et al., 2008; Ma and Yue, 2010; Yu et al., 2011; Wang et al., 2014; Chen et al., 2015; Sun et al., 2015b). There is a need to reevaluate the generation of these rocks and whether they can indicate a thickened lower crust.

Here we present new geochronology, geochemical, and isotopic data for the Gaerqiong diorite porphyries (GPs) and the Xiongma plutons (XPs) in the NW Lhasa Terrane. Our results, combined with previously published data on this region, are used to explore the following fundamental questions regarding the Cretaceous intermediate-silicic rocks in the NW Lhasa Terrane. (1) Do these intermediate-silicic rocks reflect thickening of the regional lower crust since the Cretaceous? (2) If so, how was the lower crust thickened and then uplifted?

†Corresponding author: lzdxchen@gig.ac.cn.

GSA Bulletin; January/February 2020; v. 132; no. 1/2; p. 334–352; https://doi.org/10.1130/B31915.1; 11 figures; 2 tables; Data Repository item 2019163; published online 2 May 2019.

GEOLOGY OF BACKGROUND

The Tibetan Plateau consists of the Songpan-Gangzi, Qiangtang, Lhasa, and Himalaya Terranes from north to south. The Lhasa Terrane is bounded by the Bangong-Nujiang Suture Zone (BNSZ) to the north and the Indus–Yarlung Zangbo Suture Zone (IYZSZ) to the south (Figs. 1A and 1B). The formation of the BNSZ and IYZSZ occurred mainly from the Late Jurassic to Early Cretaceous (Yin and Harrison, 2000; Pan et al., 2006) and from the Late Cretaceous to Early Paleogene (Dewey et al., 1988), respectively. Recently, the Lhasa Terrane has been subdivided into southern, central, and northern subterranes, separated by the Luobadui-Milashan Fault and Shiquan River–Nam Tso Mélange Zone (Zhu et al., 2011).

The southern Lhasa subterrane is considered to be the juvenile continental crust dominated by the Late Triassic to Eocene Gangdese batholith (205–40 Ma), the Mesozoic Yeba Formation, the Sangri Group, the Cenozoic Linzizong volcanic succession, adakites, and potassic-ultrapotassic rocks (Mo et al., 2007, 2008; Ji et al., 2009; Zhu et al., 2011, 2013). These rocks were commonly considered to be associated with the northward subduction of the Neo-Tethyan Ocean lithosphere and subsequent India-Asia collision (Yin and Harrison, 2000; Ding et al., 2003; Chung et al., 2005; Mo et al., 2007, 2008). In the southern Lhasa subterrane, the Mesozoic sedimentary cover is restricted to the eastern portion and separated from the passive continental margin sedimentary sequence in the Tethyan Himalaya by the IYZSZ (Zhu et al., 2013).

Apart from the Amdo microcontinent that comprises Cambrian or Neoproterozoic crystalline basement (Xu et al., 1985; Dewey et al., 1988), the northern Lhasa terrane is dominated by juvenile crust covered by Middle Triassic to Cretaceous sedimentary rocks along with

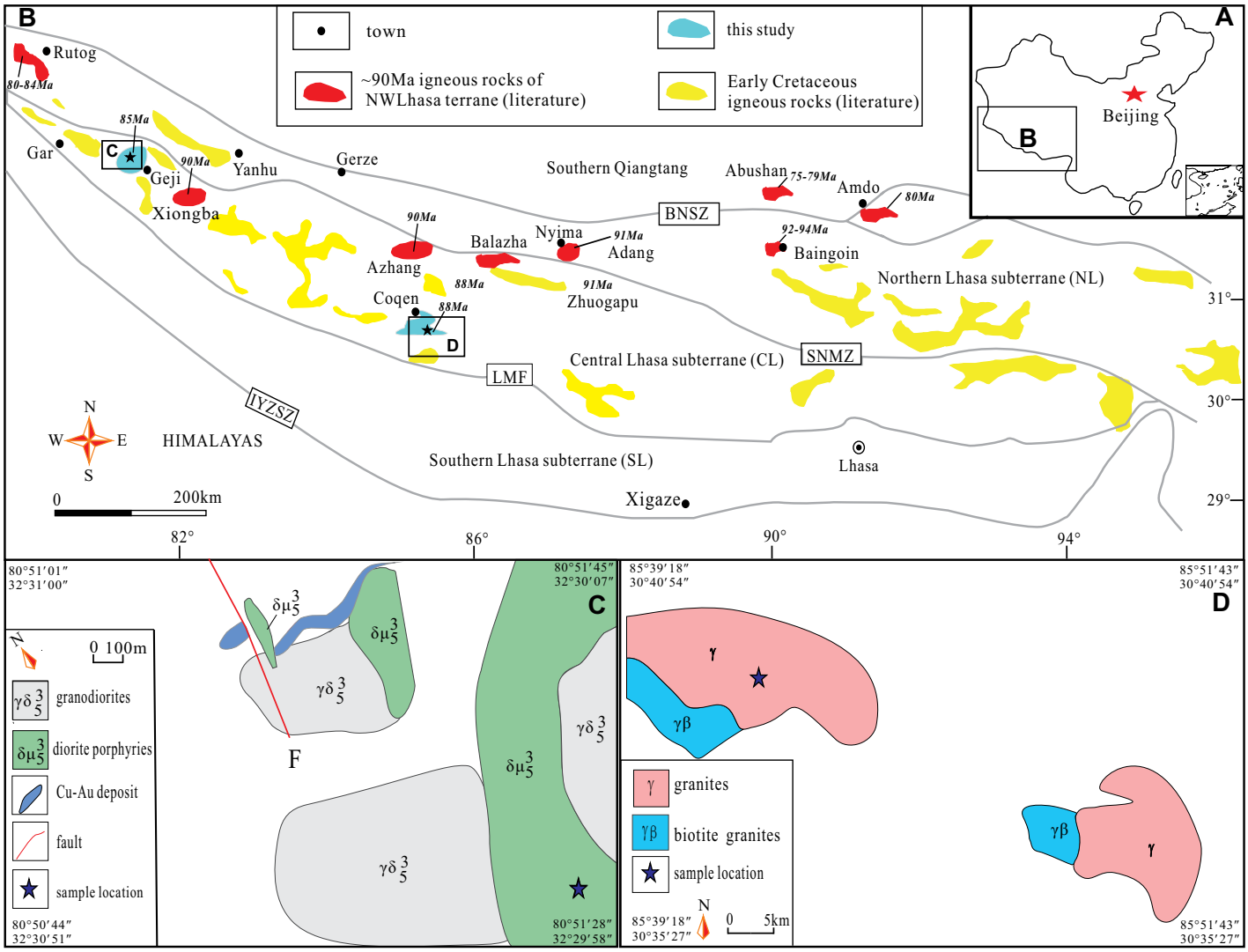

Figure 1. (A) Regional map showing the location of the Tibetan Plateau. (B) Tectonic units of the Lhasa Terrane showing the major subdivisions and distribution of magmatic rocks dated at ca. 90 Ma. (C) Geological map of the Gaerqiong Cu-Au deposit, modified from Lv (2012). (D) Geological map of the Xiongma area, modified from the 1:250,000 Coqen geological map (Jiang et al., 2002). BNSZ—Bangong-Nujiang suture zone; IYZSZ—Indus–Yarlung Zangbo Suture Zone; SNMZ—Shiquan River–Nam Tso Mélange Zone; LMF—Luobadui-Milashan Fault; F—fault. The age data of the reported Late Cretaceous (ca. 90 Ma) igneous rocks of the NW Lhasa Terrane in (B) are from Zhao et al. (2008), Ma and Yue (2010), Yu et al. (2011), Li et al. (2013), Liu et al. (2014), Wang et al. (2014), Chen et al. (2015), Liu et al. (2015), Sun et al. (2015b), S.S. Chen et al. (2017b), and Yi et al. (2018). The data of Early Cretaceous igneous rocks of the Lhasa Terrane in (B) are modified from Zhu et al. (2009).

Early Cretaceous volcanic rocks and associated granitoids (Zhu et al., 2011, 2013). The Early Cretaceous magmatism in the northern Lhasa subterrane is interpreted to have resulted from southward subduction of the Bangong-Nujiang Tethyan seafloor and continental collision between the Lhasa and Qiangtang terranes (Zhu et al., 2011, 2013; S.S. Chen et al., 2017a).

The central Lhasa subterrane underlain by Archean to Proterozoic basement may represent a micro-continent separated from east Gondwana that drifted across the Tethyan Ocean (Zhu et al., 2011). The Precambrian basement represented by the Nyainqêntanglha Group (Allègre et al., 1984; Zhu et al., 2009, 2011, 2013) has been identified in the eastern part of the central Lhasa subterrane. Recent studies have shown that this basement experienced multiple episodes of metamorphism during the Neoproterozoic, Late Triassic and Cenozoic (e.g., Zhu et al., 2013, and references therein). This reworked crystalline basement is covered by a Carboniferous metasedimentary sequence, Permian limestone, minor Jurassic siliciclastic rocks and abundant Cretaceous intrusive and volcanic rocks (Zhu et al., 2009, 2011, 2013) and minor Ordovician, Silurian, and Triassic limestones (e.g., Pan and Ding, 2004). The Late Jurassic to Early Cretaceous volcanosedimentary rocks together with the associated granitoids are abundant throughout the central Lhasa subterrane and have been attributed to the subduction and slab break-off of the Bangong-Nujiang oceanic lithosphere (Kang et al., 2008; Zhu et al., 2011, 2013). In this study, we focus on two plutons (GPs in the Geji area; XPs in the Coqen area) in the central Lhasa subterrane.

The GPs are found in the Gaerqiong skarn Cu-Au deposit, which is located in the western Geji County of the central Lhasa subterrane (Fig. 1C). The strata in this area are mainly Cretaceous quartzo-feldspathic sandstone (Duoai Formation), siltstone, limestone, marble, volcaniclastic rocks, and Quaternary sediments. The widespread intrusions related to the skarn Cu-Au deposit are mainly quartz diorites, granodiorites, and diorite porphyries (Lv, 2012; Yao et al., 2012). The studied diorite porphyries have porphyritic texture. The diorite porphyries consist of coarse euhedral-subhedral plagioclase (55%) and amphibole (35%) phenocrysts and the minor accessory minerals such as zircon and apatite. Plagioclases show narrow polysynthetic twinning and zoned textures (Fig. 2A), and some amphiboles exhibit weak zoning (Fig. 2B).

The XPs were sampled in the western Coqen area of the central Lhasa subterrane. The strata exposed in this district are the lower Permian Laga Formation and Quaternary sediments. The magmatic rocks chiefly comprise granites and biotite granites (Fig. 1D; Jiang et al., 2002). The XPs are composed of Xiongma granites and mafic microgranular enclaves (MMEs; 20–30 cm in diameter; Fig. 2C), and the MMEs make up ~5 vol% of the pluton. The lobate to cuspate contacts of MMEs against the host rocks suggest that both of them coexisted as contemporaneous magmas. The euhedral-subhedral phenocrysts in the granites are plagioclase (30%), quartz (25%), biotite (15%), and amphibole (15%) with minor amounts of accessory minerals such as zircon and apatite (Fig. 2D). The equigranular and fine-grained MMEs (e.g., sample 13XM-12) consist of hornblende (30%), biotite (30%), pyroxene (10%), plagioclase (10%), K-feldspar (10%), and quartz (5%), along with the assemblages of accessory minerals comprising titanite, magnetite, and apatite. Apatite has a euhedral and acicular habit. The enclaves contain K-feldspar megacrysts, which are texturally and compositionally identical to these in the host rocks (Figs. 2E and 2F).

ANALYTICAL METHODS

Zircon U-Pb Dating

All zircons for U-Pb dating were separated using conventional heavy liquid and magnetic separation techniques. Zircon grains were handpicked and mounted in epoxy resin, and then polished to half their thickness and coated with gold. The internal morphology of the zircons was imaged using cathodoluminescence (CL) techniques with a JEOL JXA-8100 Superprobe prior to U-Pb isotopic analysis at the Guangzhou Institute of Geochemistry, Chinese Academy of Sciences (GIG-CAS), Guangzhou, China. U-Pb dating of zircon was performed by laser ablation–inductively coupled plasma–mass spectrometry (LA-ICP-MS) at China University of Geosciences, Wuhan. For details of the analytical procedures, see Zhang et al. (2007). The zircon 91500 was used as the external standard, and NIST SRM 610 and Zr were used as the reference material and internal standard, respectively. The time-resolved spectra were analyzed off-line by ICPMSDataCal. Common Pb was corrected following the method of Andersen (2002). The Isoplot/Ex 3.0 software (Ludwig, 2003) was used for calculating U-Pb ages. Uncertainties in the ages are cited at the 1σ level and the weighted mean ages are quoted at the 95% confidence level.

Zircon Hf Isotope Analyses

Zircon Lu-Hf isotopic compositions of the GPs (13GJ-07 and 13GJ-08) were measured using a multi-collector (MC) ICP-MS (Thermo Electron Neptune) at GIG-CAS. Hf isotopic data were acquired by ablation with a 45 μm beam diameter and a laser repetition rate of 7 Hz. During the study, the average $^{176}Hf/^{177}Hf$ ratio obtained for the Penglai zircon was 0.282902 ± 0.000009 (1σ; n = 26), which is consistent with the recommended $^{176}Hf/^{177}Hf$ ratio for this standard (Li et al., 2010). The detailed analytical methods of Hf isotope are similar to these described by Zhang et al. (2015).

Zircon Lu-Hf isotopic data for the XPs (13XM-05, 13XM-10, and 13XM-12) were obtained at the Guangxi Key Laboratory of Hidden Metallic Ore Deposits Exploration, Guilin University of Technology, Guilin, China. Replicate analyses of the GJ-1 zircon standard gave a mean $^{176}Hf/^{177}Hf$ ratio of 0.282006 ± 0.000016 (2σ; n = 20), which is consistent with previous study (0.282013 ± 0.000003; Yuan et al., 2008), indicating that the interference corrections and the zircon Hf isotopic results are robust.

Whole-Rock Major- and Trace-Element Analyses

All samples were powdered in an agate mill to 200 mesh. Major-element contents were determined at GIG-CAS using a wavelength X-ray fluorescence (XRF) spectrometer. The analytical uncertainties on major elements are generally better than 5%. The detailed analytical procedures are described by Goto and Tatsumi (1994).

The trace-element analyses were performed at GIG-CAS by ICP-MS using a Perkin-Elmer Sciex ELAN 6000 instrument. For most of the trace elements, analytical precision and accuracy are better than 5%. The detailed analytical procedures are the same as described by Li et al. (2006).

Whole-Rock Sr-Nd Isotope Analyses

Whole-rock Sr and Nd isotope analyses were performed with a Micromass Isoprobe MC-ICP-MS at Guilin University of Technology and at GIG-CAS, respectively. Sr and rare earth elements (REE) were separated using cation exchange columns, and Nd fractions were further purified by HDEHP-coated columns. The $^{87}Sr/^{86}Sr$ ratio obtained for the NBS SRM 987 standard was 0.710288 ± 28 (2σ). The $^{143}Nd/^{144}Nd$ ratio obtained for the Shin Etsu JNdi-1 standard was 0.512115 ± 7 (2σ). The measured Sr and Nd isotope ratios were normalized to $^{86}Sr/^{88}Sr = 0.1194$ and $^{146}Nd/^{144}Nd = 0.7219$, respectively. Detailed procedures for Sr and Nd isotopic analyses are described by Chen et al. (2010).

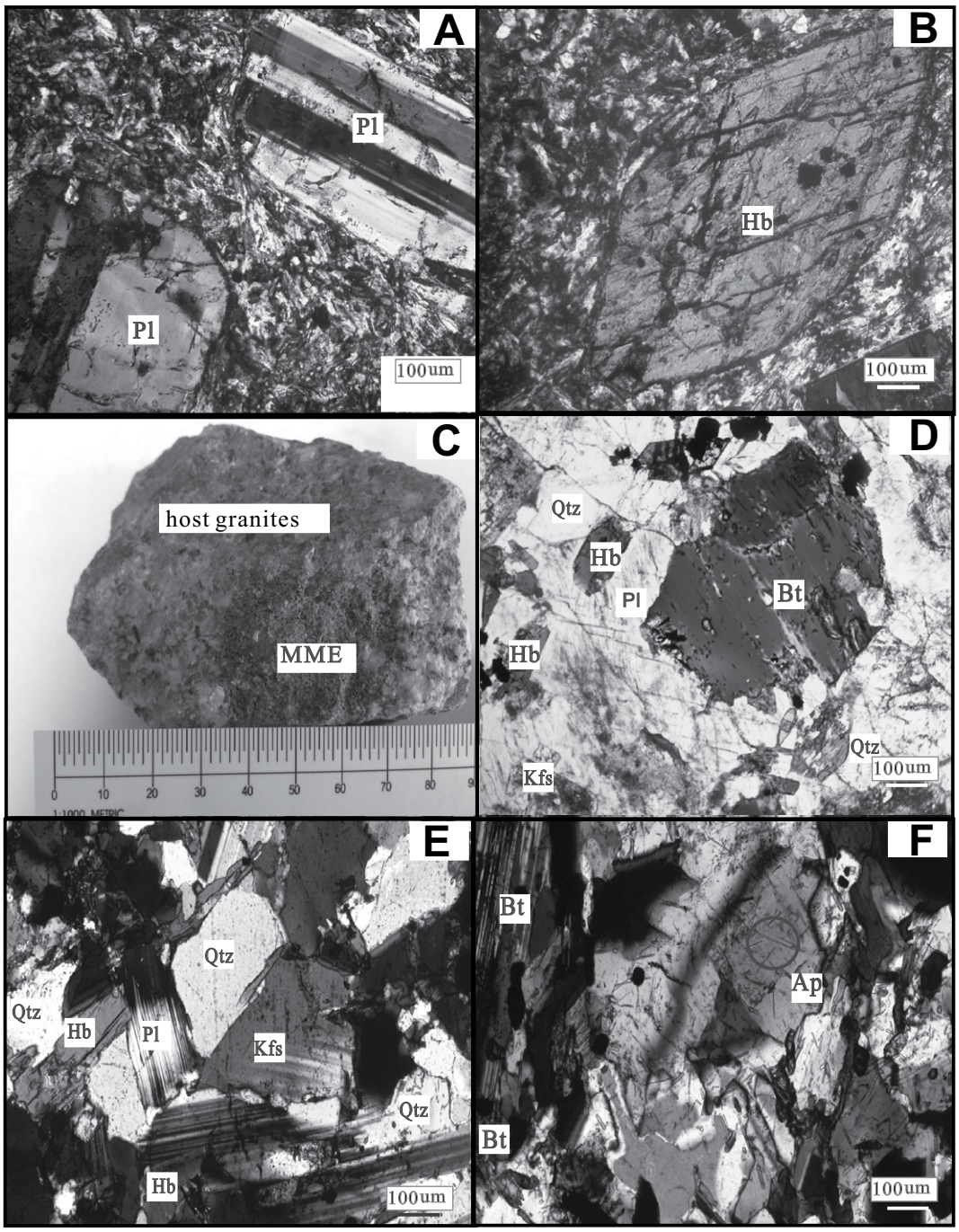

Figure 2. (A, B) Photomicrographs of porphyritic textures of the GPs (Gaerqiong diorite porphyries). (C) Hand specimen of the Xiongma pluton. (D) Photomicrograph of the Xiongma granite. (E, F) Photomicrographs of the Xiongma mafic microgranular enclaves (MMEs). Hb—hornblende; Pl—plagioclase; Bt—biotite, Kfs—K-feldspar; Ap—apatite; Qtz—quartz.

RESULTS

Zircon U-Pb Geochronology

Selected samples of the GPs (13GJ-07 and 13GJ-08) and XPs (13XM-05, 13XM-10, and 13XM-12) were dated using LA-ICP-MS. Zircon crystals from the GPs and XPs are euhedral to subhedral, and show clear oscillatory zoning in CL images and high Th/U values (typically >0.4; Fig. 3F; Supplementary Table DR1).[1] These features are consistent with an igneous origin (Koschek, 1993). Therefore, the U-Pb zircon ages represent the timing of crystallization of these magmatic rocks.

Zircon grains from GP samples 13GJ-07 and 13GJ-08 yield weighted-mean $^{206}Pb/^{238}U$ ages of 84.6 ± 1.1 Ma (mean square of weighted deviates (MSWD) = 0.17) and 84.6 ± 1.0 Ma (MSWD = 0.56), respectively (Figs. 3A and 3B; Supplementary Table DR1). Thus, the GPs were formed at ca. 84.6 Ma, which is consistent with previously published ages (90–86 Ma) for intrusive rocks of the Gaerqiong skarn Cu-Au deposit (Lv, 2012; Yao et al., 2012).

[1]GSA Data Repository item 2019163, Tables DR1–DR2, Figures DR1–DR2, Text DR1–DR2, is available at http://www.geosociety.org/datarepository/2019 or by request to editing@geosociety.org.

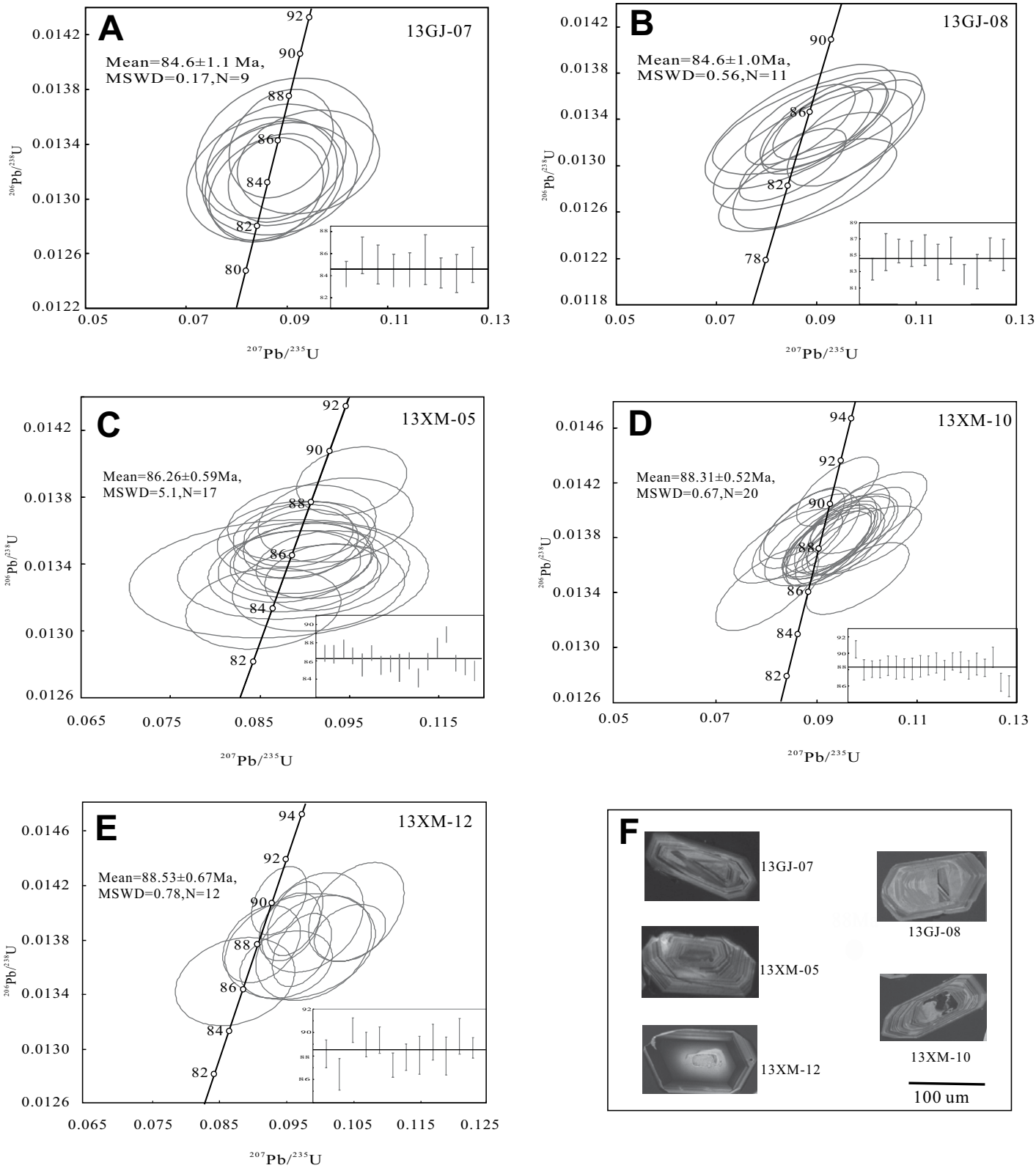

Figure 3. (A, B) Weighted-mean ages and concordia diagrams for zircons from the Gaerqiong diorite porphyries (samples 13GJ-07 and 13GJ-08). (C, D) Weighted-mean ages and concordia diagrams for zircons from the Xiongma host granites (samples 13XM-05 and 13XM-10). (E) Weighted-mean ages, concordia diagrams for zircons from the Xiongma microgranular enclaves (sample 13XM-12), and (F) cathodoluminescence images of representative zircon grains from the dated samples. Black circles indicate the sites of zircon U-Pb dating by LA-ICP-MS. MSWD—mean square of weighted deviates.

Two granite samples of the XPs (13XM-05 and 13XM-10) yield weighted-mean $^{206}Pb/^{238}U$ ages of 86.3 ± 0.6 Ma (MSWD = 5.10) and 88.3 ± 0.5 Ma (MSWD = 0.67), respectively (Figs. 3C and 3D; Supplementary Table DR1). An MME sample (13XM-12) yields a mean $^{206}Pb/^{238}U$ age of 88.5 ± 0.7 Ma (MSWD = 0.78) (Fig. 3E; Supplementary Table DR1). Thus, the Xiongma granites and MMEs crystallized coevally at ca. 88 Ma.

Whole-Rock Geochemical and Zircon Hf Isotopic Data

Whole-rock major- and trace-element, Sr-Nd isotopic, and zircon Hf isotopic data for the GPs and XPs are provided in Tables 1 and 2, respectively. The GPs have intermediate SiO_2 contents (59.50–62.99 wt%), whereas the Xiongma granites have high SiO_2 contents (65.95–68.43 wt%). Both the GPs and Xiongma granites have high alkali contents ($Na_2O + K_2O > 5.6$ wt%) and low A/CNK values (<1.1; where A/CNK refers to the molecular ratio of $Al_2O_3/(CaO + Na_2O + K_2O)$), and they belong to the aluminous to slightly peraluminous calc-alkaline series (Figs. 4A–4C). The MMEs from the XPs, however, have low SiO_2 contents (48.90–52.76 wt%) and relatively high Mg-numbers ($Mg^{\#}$ = 47–49; where $Mg^{\#} = 100 \times Mg^{2+}/(Mg^{2+} + TFe^{2+})$, and TFeO = $0.8998 \times TFe_2O_3$) and MgO values (4.47–4.65 wt%). On the chondrite-normalized rare earth element (REE) diagram (Fig. 5A), both GPs and XPs (granites and MMEs) show strong light REE (LREE) enrichment relative to the heavy REEs (HREE). On the primitive-mantle-normalized trace element diagram (Fig. 5B), they are enriched in large ion lithophile elements (LILEs; e.g., Rb and U) and depleted in high field strength elements (HFSEs; e.g., Nb, Ta, and Ti).

The dated zircons from the GPs have $^{176}Hf/^{177}Hf_{(t)}$ ratios of 0.282866–0.282999, with corresponding $\varepsilon Hf_{(t)}$ values of +5.2 to +9.9 (Fig. 6A). The GPs show limited variation in whole-rock $^{87}Sr/^{86}Sr_{(i)}$ (0.705103–0.705259) and $\varepsilon Nd_{(t)}$ (+1.7 to +2.0) isotopic compositions. The Sr-Nd isotopic compositions of the GPs are comparable to those of the Rutog adakitic rocks ($^{87}Sr/^{86}Sr_{(i)}$ = 0.7045–0.7049, $\varepsilon Nd_{(t)}$ = +0.1 to +2.3; Zhao et al., 2008), and are slightly more enriched than the Azhang adakitic rocks ($\varepsilon Hf_{(t)}$ = +8.9 to +12, $^{87}Sr/^{86}Sr_{(i)}$ = 0.7054–0.7062, $\varepsilon Nd_{(t)}$ = +2.5 to +5.6; Sun et al., 2015b), but more depleted than the ancient basement of the central Lhasa subterrane (Fig. 6B; Zhu et al., 2011). Compared with the GPs, the Xiongma granites have high $^{87}Sr/^{86}Sr_{(i)}$ (0.710589–0.711073), low $\varepsilon Nd_{(t)}$ (–7.4 to –6.3) values, and zircon $^{176}Hf/^{177}Hf_{(t)}$ ratios of 0.282408–0.282601, with corresponding $\varepsilon Hf_{(t)}$ values of –11.0 to –4.1 (Fig. 6A). The Sr-Nd isotopic compositions of the Xiongma granites are comparable to previously published data of the Coqen granites ($^{87}Sr/^{86}Sr_{(i)}$ = 0.70874–0.70944, $\varepsilon Nd_{(t)}$ = –7.5 to –6.8; Qu et al., 2006; Xin et al., 2007), but are much higher than those of the ancient basement of the central Lhasa subterrane (Fig. 6B; Zhu et al., 2011). The $^{176}Hf/^{177}Hf_{(t)}$ ratios of zircons from the Xiongma MMEs are 0.282323–0.282553, with corresponding $\varepsilon Hf_{(t)}$ values of –14.0 to –5.8.

TABLE 1. MAJOR-(WT%), TRACE ELEMENT (PPM) AND Sr–Nd ISOTOPIC DATA FOR SAMPLES OF GAERQIONG DIORITE PORPHYRIES AND XIONGMA PLUTONS

Sample	13GJ-7	13GJ-8	13GJ-9	13GJ-10	13GJ-11	13GJ-12
SiO_2	60.63	59.5	62.37	62.99	62.67	61.16
TiO_2	0.77	0.84	0.71	0.71	0.76	0.75
Al_2O_3	14.70	14.77	14.98	14.83	14.81	14.71
Fe_2O_3	4.16	4.29	3.76	3.89	4.47	3.33
MnO	0.15	0.13	0.11	0.10	0.16	0.12
MgO	4.24	4.86	3.61	3.68	3.56	3.61
CaO	6.97	7.73	6.14	5.73	6.15	7.49
Na_2O	3.55	3.59	4.45	3.68	3.83	3.65
K_2O	3.14	1.96	2.41	3.10	2.29	3.16
P_2O_5	0.24	0.27	0.22	0.22	0.24	0.24
LOI	1.09	1.77	0.87	0.80	0.77	1.49
A/CNK	0.91	0.91	1.09	1.07	1.08	0.86
A/NK	4.32	6.95	5.72	4.41	5.97	4.29
Mg#	67	69	66	65	61	68
Sc	11.6	12.3	12.2	11.9	11.7	11.6
Cr	153	205	197	153	208	175
Ni	70.1	80.4	74.2	70.3	70	74.4
Ga	16.5	16.9	16.6	16.9	16.8	16.9
Rb	101	51.3	76.7	90.3	70.6	92.1
Sr	413	427	406	418	411	428
Y	12.4	12.4	11.8	11.7	11.7	12.1
Zr	154	168	160	155	175	181
Nb	13.6	13.7	11.8	12.0	12.1	13.7
Cs	3.52	4.08	5.57	3.06	4.27	4.61
Ba	392	321	382	383	378	414
La	27.9	23.0	26.4	24.8	32.0	26.8
Ce	54.2	48.4	51.1	51.9	60.8	51.4
Pr	5.93	5.63	5.48	5.75	6.20	5.52
Nd	21.7	21.1	19.9	20.8	21.4	20.5
Sm	3.70	3.76	3.51	3.59	3.50	3.50
Eu	1.04	1.08	1.04	1.07	1.07	0.98
Gd	3.20	3.21	3.24	3.31	3.02	3.06
Tb	0.45	0.46	0.46	0.46	0.46	0.43
Dy	2.42	2.51	2.40	2.39	2.34	2.33
Ho	0.48	0.50	0.48	0.47	0.46	0.46
Er	1.25	1.30	1.25	1.26	1.26	1.23
Tm	0.18	0.19	0.18	0.18	0.19	0.18
Yb	1.14	1.16	1.18	1.17	1.20	1.14
Lu	0.18	0.18	0.18	0.18	0.18	0.18
Hf	3.73	4.04	3.85	3.75	4.09	4.30
Ta	1.00	0.99	0.94	0.97	0.94	1.01
Pb	8.89	11.1	10.8	7.87	7.73	9.51
Th	8.99	8.33	8.60	8.73	8.63	9.14
U	2.13	1.2	2.05	2.06	2.15	2.38
δEu	0.92	0.95	0.94	0.95	1.01	0.92
Sr/Y	33.3	34.3	34.5	35.8	35.2	35.1
Tzr (°C)	------	--------	------	--------	------	--------
Cr/Th	17.0	24.6	22.9	17.5	24.1	19.1
Sr/Ba	1.1	1.3	1.1	1.1	1.1	1.0
Zr+Nb+Ce+Y	234.2	242.5	234.7	230.6	259.6	258.3
10,000Ga/Al	2.1	2.2	2.1	2.2	2.1	2.2
$^{87}Sr/^{86}Sr$	0.706040	0.705549	0.705738	0.705881	0.705836	0.705904
2σ	0.000008	0.000016	0.000014	0.000006	0.000016	0.000011
$^{87}Sr/^{86}Sr_{(i)}$	0.705221	0.705146	0.705103	0.705156	0.705259	0.705182
$^{143}Nd/^{144}Nd$	0.51269	0.51268	0.512684	0.512684	0.512674	0.512672
2σ	0.000007	0.000009	0.000007	0.000008	0.000007	0.000008
$^{143}Nd/^{144}Nd_{(t)}$	0.512631	0.512619	0.512624	0.512625	0.512618	0.512614
$\varepsilon Nd_{(t)}$	2.00	1.76	1.85	1.88	1.74	1.66

(*continued*)

PETROGENESIS

Petrogenesis of the Gaerqiong Diorite Porphyries

The GPs exhibit some adakitic affinities, such as high contents of SiO_2 (>59.50 wt%), Sr (>405 ppm), Sr/Y ratios (>33) and low Y (<13 ppm) values. Meanwhile, they have high MgO (3.56–4.86 wt%), Cr (>150 ppm), Ni (>70 ppm), and $Mg^{\#}$ (61–69) values. The GPs, therefore, can be described as high-$Mg^{\#}$ adakitic rocks (Figs. 7A–7D).

TABLE 1. MAJOR-(WT%), TRACE ELEMENT (PPM) AND Sr–Nd ISOTOPIC DATA FOR SAMPLES OF GAERQIONG DIORITE PORPHYRIES AND XIONGMA PLUTONS (*continued*)

Sample	13XM-01	13XM-02	13XM-03	13XM-04	13XM-05	13XM-06	13XM-07	13XM-08	13XM-09	13XM-10	13XM-11	13XM-12	13XM-13
SiO_2	66.37	67.89	66.33	65.95	67.78	68.43	67.56	68.35	66.23	67.12	67.06	52.76	48.90
TiO_2	0.52	0.45	0.50	0.53	0.45	0.45	0.50	0.38	0.53	0.51	0.51	1.10	1.30
Al_2O_3	15.53	14.90	15.45	15.56	15.27	14.64	15.04	15.04	15.45	14.90	15.25	17.06	17.75
Fe_2O_3	4.43	3.38	4.49	4.22	3.84	3.83	4.23	3.43	4.53	4.31	4.26	9.52	9.94
MnO	0.14	0.08	0.16	0.15	0.11	0.13	0.13	0.12	0.13	0.14	0.14	0.30	0.24
MgO	1.54	1.25	1.47	1.48	1.32	1.29	1.49	1.17	1.50	1.45	1.55	4.65	4.47
CaO	3.16	3.26	3.52	3.47	3.22	3.24	3.42	3.14	3.60	2.81	3.45	6.46	6.83
Na_2O	3.39	3.18	3.30	3.47	3.32	3.03	3.21	3.32	3.33	3.28	3.27	3.70	4.24
K_2O	3.58	4.03	3.86	3.52	3.71	3.79	3.61	3.87	3.60	3.79	3.52	2.70	1.71
P_2O_5	0.15	0.17	0.15	0.16	0.14	0.14	0.15	0.12	0.16	0.15	0.15	0.27	0.30
LOI	0.98	0.83	0.83	1.17	0.66	0.47	0.73	0.88	0.78	1.52	0.90	1.50	3.80
A/CNK	1.02	0.96	0.96	0.98	0.99	0.98	0.98	0.98	0.97	1.02	0.99	0.82	0.83
A/NK	1.64	1.55	1.61	1.63	1.61	1.61	1.64	1.56	1.65	1.57	1.66	1.89	2.01
Mg#	41	42	40	41	41	40	41	40	40	40	42	49	47
Sc	6.24	6.69	6.26	6.21	5.62	5.71	5.68	4.98	6.03	5.99	6.29	25.2	24.1
Cr	21.7	6.33	89.1	9.75	17.6	9.29	16.3	15.0	18.0	9.65	16.1	39.7	18.3
Ni	5.00	3.50	4.97	4.04	3.46	3.48	4.05	3.47	3.86	4.10	4.24	7.87	9.31
Ga	19.0	16.5	18.1	17.9	17.1	16.7	16.7	16.5	18.5	17.5	18.0	24.7	28.2
Rb	150	160	149	140	143	148	132	130	137	158	136	170	117
Sr	468	371	432	456	424	404	405	467	438	392	432	369	567
Y	14.7	16.8	14.0	14.3	13.1	12.8	13.0	10.2	16.5	14.0	15.1	32.7	32.5
Zr	117	137	115	131	101	111	104	98.2	128	145	123	108	106
Nb	11.3	11.3	10.4	11.1	10.1	9.88	9.79	7.62	12.0	10.9	11.1	22.4	28.5
Cs	3.42	3.07	2.57	2.18	3.15	2.61	2.50	3.93	3.36	3.24	2.93	3.45	2.22
Ba	490	501	544	511	440	500	476	570	485	520	472	296	261
La	26.9	33.3	27.9	39.3	21.3	19.4	23.2	17.3	35.7	21.5	30.1	26.9	30.7
Ce	56.8	62.0	55.5	70.6	45.6	41.4	47.9	36.0	66.8	46.5	57.4	69.8	76.0
Pr	6.37	7.18	6.55	7.70	5.56	5.20	5.60	4.34	7.74	5.79	6.77	10.5	11.0
Nd	23.3	25.5	24.0	26.6	20.7	19.7	20.5	16.1	27.6	21.6	24.6	42.1	42.4
Sm	4.21	4.51	4.31	4.56	3.89	3.65	3.72	2.96	4.90	4.06	4.38	8.29	8.33
Eu	1.07	1.04	1.06	1.07	0.99	0.94	0.94	0.86	1.14	1.02	1.05	1.69	1.81
Gd	3.60	3.84	3.55	3.77	3.23	3.11	3.15	2.50	4.14	3.43	3.73	7.06	7.23
Tb	0.48	0.53	0.48	0.50	0.44	0.43	0.43	0.34	0.56	0.47	0.50	1.01	1.02
Dy	2.64	2.87	2.60	2.67	2.42	2.32	2.31	1.85	2.99	2.55	2.74	5.72	5.67
Ho	0.51	0.57	0.50	0.52	0.48	0.45	0.45	0.36	0.58	0.50	0.53	1.16	1.13
Er	1.37	1.57	1.33	1.37	1.25	1.20	1.21	0.97	1.52	1.34	1.41	3.16	3.06
Tm	0.20	0.24	0.20	0.20	0.19	0.18	0.18	0.14	0.23	0.20	0.21	0.48	0.46
Yb	1.34	1.59	1.31	1.36	1.25	1.22	1.22	0.95	1.49	1.32	1.40	3.24	3.06
Lu	0.21	0.26	0.21	0.22	0.19	0.19	0.19	0.15	0.23	0.21	0.22	0.52	0.49
Hf	3.24	3.89	3.19	3.68	2.96	3.08	2.92	2.74	3.61	4.10	3.58	3.35	3.27
Ta	1.07	1.17	1.01	1.06	1.00	0.96	0.95	0.75	1.22	1.02	1.09	2.03	2.04
Pb	16.8	23.1	31.6	21.2	14.4	18.2	19.1	15.7	16.5	18.9	16.2	13.6	22.6
Th	15.4	20.9	14.4	17.0	9.60	12.0	13.5	10.0	16.1	15.3	25.2	8.06	7.81
U	3.74	5.15	3.55	3.35	2.51	3.20	3.27	2.84	3.15	3.79	5.71	3.54	4.88
δEu	0.84	0.76	0.83	0.79	0.85	0.85	0.84	0.97	0.77	0.84	0.79	0.68	0.71
Sr/Y	32.0	22.2	31.0	31.8	32.5	31.7	31.1	45.6	26.6	28.0	28.7	11.3	17.4
Tzr (°C)	750	758	741	754	737	744	736	734	750	769	750	-	-
Cr/Th	1.4	0.3	6.2	0.6	1.8	0.8	1.2	1.5	1.1	0.6	0.6	4.9	2.3
Sr/Ba	1.0	0.7	0.8	0.9	1.0	0.8	0.9	0.8	0.9	0.8	0.9	1.2	2.2
Zr+Nb+Ce+Y	200.2	227.0	194.7	226.8	170.1	175.5	174.3	152.0	222.9	216.8	206.6	232.7	243.2
10,000Ga/Al	2.3	2.1	2.2	2.2	2.1	2.2	2.1	2.1	2.3	2.2	2.2	2.7	3.0
$^{87}Sr/^{86}Sr$	0.711816	-	-	-	0.711902	0.712080	0.711827	0.711564	0.711745	0.712471	-	-	-
2σ	0.000008	-	-	-	0.000010	0.000010	0.000007	0.000010	0.000008	0.000010	-	-	-
$^{87}Sr/^{86}Sr_{(t)}$	0.710701	-	-	-	0.710721	0.710799	0.710688	0.710589	0.710651	0.711073	-	-	-
$^{143}Nd/^{144}Nd$	0.512246	-	-	-	0.512241	0.512248	0.512247	0.512239	0.512267	0.512210	-	-	-
2σ	0.000007	-	-	-	0.000007	0.000007	0.000007	0.000008	0.000010	0.000008	-	-	-
$^{143}Nd/^{144}Nd_{(t)}$	0.512182	-	-	-	0.512174	0.512182	0.512182	0.512174	0.512204	0.512143	-	-	-
$\varepsilon Nd_{(t)}$	–6.68	-	-	-	–6.84	–6.68	–6.67	–6.84	–6.26	–7.44	-	-	-

Note: LOI—loss of ignition. ACNK = $Al_2O_3/(Ca_2O + Na_2O + K_2O)$. ANK = $Al_2O_3/(Na_2O + K_2O)$. δEu =2 $Eu_N/(Sm_N \times Gd_N)$, N denotes chondrite normalization. Major and trace element data of GPs are from Lei et al. (2015); other data are from this study. Samples of 13XM-12 and 13XM-13 are mafic microgranular enclaves (MMEs); other samples of XPs are granites. Zircon saturation temperature is calculated by using the method of Watson and Harrison (1983). The calculation of initial whole rock Sr-Nd and zircon Hf isotopic values is given in the Supplementary Text DR1 (see footnote 1).

Previous studies have proposed the following mechanisms for the formation of high-Mg# adakitic rocks. (1) Partial melting of a young and hot subducted oceanic crust (Defant and Drummond, 1990). (2) Partial melting of lithospheric mantle sources enriched by fluids or melts from a subducted slab (Shirey and Hanson, 1984; Shimoda et al., 1998). (3) Mixing between mantle- and crust-derived melts (Guo et al., 2007; Streck et al., 2007). (4) High-pressure fractional crystallization (FC) or low-pressure assimilation and fractional crystallization (AFC) of basaltic magmas (Castillo et al., 1999; Macpherson et al., 2006). (5) Partial melting of the delaminated lower continental crust (Xu et al., 2002; Gao et al., 2004; Wang et al., 2006).

Typical adakites formed by partial melting of a subducted oceanic slab have high Na_2O (mostly $Na_2O/K_2O > 0.4$), low Th (<3 ppm), and mid-oceanic ridge basalt (MORB)-like Sr-Nd isotopic compositions (Defant and Drummond, 1990). However, the GPs have high K_2O ($Na_2O/K_2O < 0.4$) and Th (>8 ppm) contents with Sr-Nd isotopic values distinct from those of Meso-Tethyan oceanic crust (Fig. 6B). Moreover, the closure of the Bangong-Nujiang Tethys Ocean occurred primarily during the Late Jurassic to Early Cretaceous (Zhu et al., 2009, 2011, 2013). Therefore, the Late Cretaceous GPs are unlikely to be related to partial melting of the

TABLE 2. IN SITU ZIRCON Hf ISOTOPIC DATA FOR SAMPLES OF GAERQIONG DIORITE PORPHYRIES AND XIONGMA PLUTONS

Sample no.	Age (Ma)	$^{176}Yb/^{177}Hf$	$^{176}Lu/^{177}Hf$	$^{176}Hf/^{177}Hf$	2σ	$^{176}Hf/^{177}Hf_{(t)}$	$\varepsilon Hf_{(t)}$	T_{DM} (Ma)	T_{DM}^{C} (Ma)
13GJ-07									
13GJ-07-2	84.6	0.027147	0.000991	0.282896	1	0.282895	6.2	505	756
13GJ-07-3	84.6	0.024195	0.000854	0.282935	7	0.282933	7.6	448	668
13GJ-07-11	84.6	0.018792	0.000670	0.282951	8	0.282950	8.1	424	632
13GJ-07-14	84.6	0.028397	0.000997	0.282943	9	0.282942	7.9	438	649
13GJ-07-16	84.6	0.018737	0.000666	0.283000	8	0.282999	9.9	354	519
13GJ-07-17	84.6	0.030978	0.001026	0.282974	9	0.282973	9.0	394	579
13GJ-07-18	84.6	0.033051	0.001079	0.282946	14	0.282945	8.0	435	643
13GJ-07-20	84.6	0.018410	0.000663	0.282928	7	0.282927	7.3	455	683
13GJ-07-21	84.6	0.023574	0.000794	0.282992	8	0.282991	9.6	366	537
13GJ-08									
13GJ-08-02	84.6	0.019885	0.000655	0.282983	7	0.282982	9.3	378	557
13GJ-08-03	84.6	0.020967	0.000727	0.282899	8	0.282898	6.3	497	748
13GJ-08-07	84.6	0.034714	0.001112	0.282956	8	0.282954	8.3	422	622
13GJ-08-08	84.6	0.024388	0.000828	0.282971	8	0.282970	8.8	397	586
13GJ-08-10	84.6	0.025926	0.000958	0.282889	13	0.282888	6.0	514	771
13GJ-08-12	84.6	0.035434	0.001144	0.282952	9	0.282950	8.2	427	630
13GJ-08-14	84.6	0.027327	0.000874	0.282867	1	0.282866	5.2	544	822
13GJ-08-17	84.6	0.024746	0.000819	0.282938	9	0.282936	7.7	444	662
13GJ-08-18	84.6	0.027857	0.000977	0.282973	7	0.282971	8.9	396	582
13GJ-08-20	84.6	0.037374	0.001212	0.282951	8	0.282949	8.1	430	633
13GJ-08-23	84.6	0.032744	0.001069	0.282897	8	0.282895	6.2	505	755
13XM-05									
13XM5-01	88	0.0276484	0.0009005	0.282514	15	0.282513	–7.2	1042	1617
13XM-5-02	88	0.0299539	0.0009857	0.282493	15	0.282491	–8.0	1074	1665
13XM-5-04	88	0.0240766	0.0009428	0.282530	13	0.282528	–6.7	1021	1582
13XM-5-07	88	0.1101829	0.0036271	0.282500	23	0.282490	–7.9	1144	1657
13XM-5-12	88	0.0470743	0.0018907	0.282529	18	0.282526	–6.8	1048	1586
13XM-5-15	88	0.0305243	0.0010441	0.282510	16	0.282508	–7.4	1052	1627
13XM-5-17	88	0.0256668	0.0008354	0.282517	17	0.282515	–7.1	1037	1611
13XM-5-18	88	0.0423107	0.001330	0.282561	14	0.282558	–5.6	988	1514
13XM-5-19	88	0.0127418	0.0004652	0.282576	16	0.282575	–5.0	945	1477
13XM-5-20	88	0.028614	0.0009376	0.282502	15	0.282500	–7.7	1060	1645
13XM-5-22	88	0.027762	0.000941	0.282602	18	0.282601	–4.1	919	1419
13XM-5-23	88	0.0363112	0.0012338	0.282565	18	0.282563	–5.5	979	1504
13XM-10									
13XM-10-4	88	0.0274399	0.0010866	0.282520	16	0.282518	–7.1	1039	1605
13XM-10-5	88	0.0277145	0.0009208	0.282518	14	0.282516	–7.1	1038	1609
13XM-10-7	88	0.0265607	0.0009257	0.282517	15	0.282516	–7.1	1038	1610
13XM-10-8	88	0.0331143	0.0011966	0.282512	16	0.282510	–7.3	1053	1622
13XM-10-11	88	0.0317086	0.001140	0.282576	17	0.282574	–5.1	961	1479
13XM-10-12	88	0.0241076	0.0008937	0.282502	14	0.282500	–7.7	1060	1645
13XM-10-13	88	0.0292774	0.0009875	0.282531	16	0.282529	–6.7	1021	1579
13XM-10-14	88	0.0241293	0.0008493	0.282409	18	0.282408	–11.0	1187	1852
13XM-10-15	88	0.0382809	0.0011698	0.282490	13	0.282488	–8.1	1084	1672
13XM-10-16	88	0.0270303	0.0009407	0.282548	16	0.282547	–6.0	995	1540
13XM-10-17	88	0.0280175	0.0009772	0.282544	17	0.282543	–6.2	1002	1549
13XM-10-18	88	0.0883385	0.0029625	0.282532	20	0.282527	–6.7	1076	1584
13XM-10-20	88	0.0333978	0.001186	0.282477	16	0.282475	–8.6	1102	1700
13XM-10-21	88	0.0248121	0.0008667	0.282535	17	0.282533	–6.5	1012	1571
13XM-10-22	88	0.0210657	0.0007215	0.282481	14	0.282480	–8.4	1083	1690
13XM-10-24	88	0.0245107	0.0009067	0.282546	17	0.282545	–6.1	997	1544
13XM-12									
13XM-12-1	88	0.0596017	0.0025338	0.282557	34	0.282553	–5.8	1026	1526
13XM-12-3	88	0.1184343	0.0044731	0.282528	26	0.282521	–6.9	1128	1596
13XM-12-5	88	0.1185215	0.0045584	0.282493	22	0.282485	–8.2	1186	1677
13XM-12-7	88	0.0601509	0.0019154	0.282492	18	0.282489	–8.1	1102	1669
13XM-12-8	88	0.0369485	0.0013816	0.282528	24	0.282526	–6.8	1036	1587
13XM-12-9	88	0.1578832	0.0055267	0.282472	23	0.282463	–9.0	1254	1727
13XM-12-11	88	0.0631439	0.0021446	0.282545	18	0.282542	–6.2	1032	1551
13XM-12-13	88	0.0381420	0.0015719	0.282504	18	0.282502	–7.6	1075	1641
13XM-12-17	88	0.0454943	0.0017183	0.282453	18	0.282450	–9.5	1153	1757
13XM-12-19	88	0.0282460	0.0011486	0.282462	22	0.282460	–9.1	1123	1735
13XM-12-23	88	0.0359592	0.0013280	0.282325	17	0.282323	–14.0	1322	2042

Note: Sample of 13XM-12 is mafic microgranular enclaves (MME) and other samples of XPs are granites. The calculation of initial zircon Hf isotopic values is given in the Supplementary Text DR1 (see text footnote 1).

subducted Bangong-Nujiang oceanic crust. In addition, the SiO_2 contents of the GPs do not match those of the low-SiO_2 adakites (LSA), which were directly derived from lithospheric mantle enriched by previous fluids or melts from a subducted slab (Fig. 8A; Martin et al., 2005).

Adakites that were formed by the FC of basaltic magmas usually display a positive trend on a Dy/Yb (or La/Yb) versus SiO_2 diagram (Macpherson et al., 2006), which is not the case for the GPs (Figs. 8B and 8C). The GPs have limited variations in Sr-Nd isotopic values (Figs. 8D and 8E) and no negative Eu anomalies, indicating that they were not formed by AFC of basaltic magmas. In addition, the La/Yb versus La diagram (Fig. 8F) shows that partial melting, rather than FC, played a key role in the formation of the GPs.

The absence of MMEs in the GPs, combined with the limited variations in their whole-rock $^{87}Sr/^{86}Sr_{(i)}$ and $\varepsilon Nd_{(t)}$ values (Figs. 8C and 8D), imply that mixing between mantle- and crust-derived magmas is unlikely to have played a significant role in their genesis. Moreover, if the GPs were the result of mixing between mantle- and crust-derived magmas, the most likely mantle-derived magmas are represented by the parental magmas of the ca. 130 Ma Dongco basalt ($^{87}Sr/^{86}Sr_{(i)}$ = 0.7043, $\varepsilon Nd_{(t)}$ = 4.5; Wang et al., 2016a) from the BNSZ, and the crust-derived magmas are represented by the parental magmas of the strongly peraluminous S-type granite ($^{87}Sr/^{86}Sr_{(i)}$ = 0.7402, $\varepsilon Nd_{(t)}$ = –15.4; Zhu et al., 2011) from the central Lhasa subterrane. The modeling results show that the Sr-Nd isotopic values of the GPs require the addition of >90% mafic material (Fig. 9). However, the addition of such a high proportion of mafic material into a magmatic system would result in the formation of basaltic magmas, rather than the intermediate magmas of the GPs. Thus, the above lines of evidence do not support a mixing process in the petrogenesis of the GPs.

Sun et al. (2015b) showed that the Azhang adakitic rocks were produced by partial melting of thickened lower crust. As discussed above, the GPs show adakitic affinities and have $\varepsilon Nd_{(t)}$ and zircon $\varepsilon Hf_{(t)}$ values similar to those of the Azhang adakitic rocks, which imply that GPs may also have originated from such thickened lower crust. However, compared with the Azhang adakitic rocks, the GPs have high MgO (>3.56 wt%), Cr (>150 ppm), and Ni (>70 ppm) concentrations, which indicate that the parental magmas of the GPs had an input of mantle material. The GPs plotted within the field of typical delaminated lower-crust-derived high-$Mg^{\#}$ adakites on diagrams of MgO, Cr, and Ni versus SiO_2 (Figs. 7A–7C). We, thus, suggest that the GPs were most likely formed by partial melting of delaminated lower crust, as the delaminated lower crust into the asthenospheric mantle can form adakitic melts, which would interact with the mantle peridotite. When the amount of adakitic melts or local melt/rock ratio is large enough, the adakitic melts cannot be fully consumed by the surrounding mantle peridotite. Adding mantle minerals (mantle olivines) into such high amount of adakitic melts could significantly increase their MgO, Cr, and Ni contents, but does not change their incompatible element ratios (Sr/Y) or isotopic

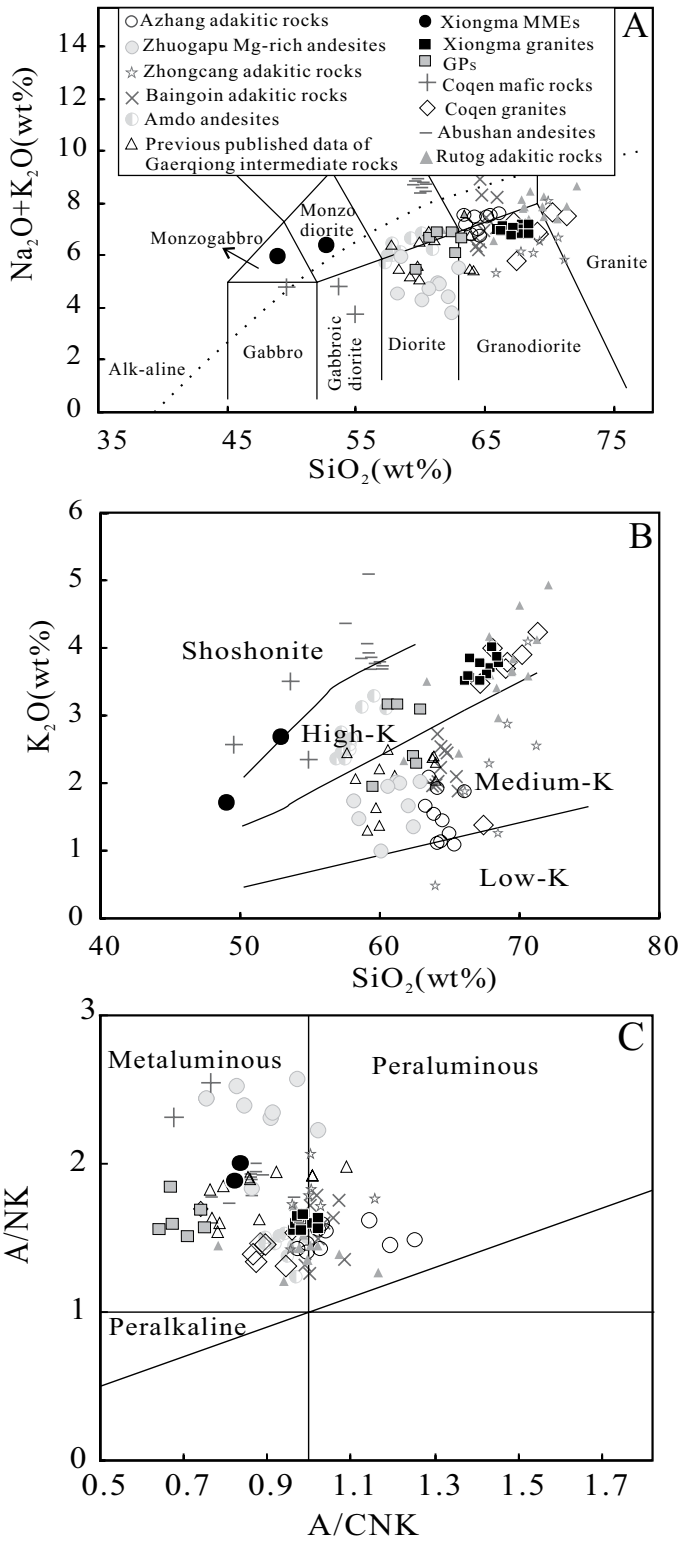

Figure 4. (A) Total alkalis versus silica diagram (after Wilson, 1989). (B) K_2O versus SiO_2 diagram (after Rollinson, 1993). (C) A/NK [$AL_2O_3/(Na_2O + K_2O)$] versus A/CNK [$AL_2O_3/(CaO + Na_2O + K_2O)$]) diagram (after Maniar and Piccoli, 1989). Data sources are as follows: Azhang adakites are from Sun et al. (2015b); Zhuogapu Mg-rich volcanic rocks are from Wang et al. (2014); Abushan andesites are from Li et al. (2013); Amdo andesites are from S.S. Chen et al. (2017b); Baingoin adakitic rocks are from Yi et al. (2018); Zhongcang adakitic porphyries are from Yu et al. (2011) and Chen et al. (2015); Rutog adakitic rocks are from Zhao et al. (2008) and Liu et al. (2015); Coqen mafic rocks and granites are from Qu et al. (2006) and Xin et al. (2007); and Gaerqiong intermediate non-adakitic rocks are from Lv (2012), and Yao et al. (2012).

compositions, and produces high-Mg# adakites such as the GPs (Rapp and Watson, 1995; Rapp et al., 1999).

However, the GPs have higher whole-rock $\varepsilon Nd_{(t)}$ and zircon $\varepsilon Hf_{(t)}$ values, and lower $^{87}Sr/^{86}Sr_{(i)}$ isotopic values than the ancient central Lhasa subterrane (Figs. 6A and 6B). There are two possible explanations for the isotopic values of the GPs: (1) the parental magmas of the GPs were derived from the ancient lower crust of the central Lhasa subterrane and then significantly modified by mantle peridotite (Chen et al., 2015); or (2) the GPs were generated from juvenile mafic lower crust that existed beneath the ancient central Lhasa subterrane (Wang et al., 2014; Sun et al., 2015b).

The results of the above Sr-Nd isotopic modeling do not support the first hypothesis (Fig. 9). Therefore, the depleted $\varepsilon Nd_{(t)}$ and $\varepsilon Hf_{(t)}$ isotopic compositions of the GPs most likely reflect the features of their continental basaltic protolith (e.g., juvenile lower crust beneath the central Lhasa subterrane; Sun et al., 2015b). As such, we suggest that the GPs were produced by partial melting of the delaminated juvenile lower crust, and the resulting melts then interact with the surrounding mantle peridotite. The intermediate rocks (diorites, quartz diorites, and granodiorites) in the Gaerqiong area showed no adakitic affinities and probably were resulted from the mixing of juvenile crust-derived melts and mantle-derived melts (Lv, 2012; Yao et al., 2012). The latter would have diluted the adakitic affinity of the former, decreasing their SiO_2 contents and zircon $\varepsilon Hf_{(t)}$ values, but increasing their MgO values (Figs. 6A and 7A–7D).

Petrogenesis of the Xiongma Pluton

Petrogenesis of MMEs

MMEs in granitoids are normally considered to be restites (Chappell et al., 1987; Chappell and White, 1991), accumulations of early formed co-genetic crystals (e.g., Bonin, 1991; Schonenberger et al., 2006), or remnants of a mafic component added to intermediate-silicic magma chambers (e.g., Holden et al., 1987; Yang et al., 2006). The Xiongma MMEs are ellipsoidal, spindle-shaped, or elongate, and exhibit typical

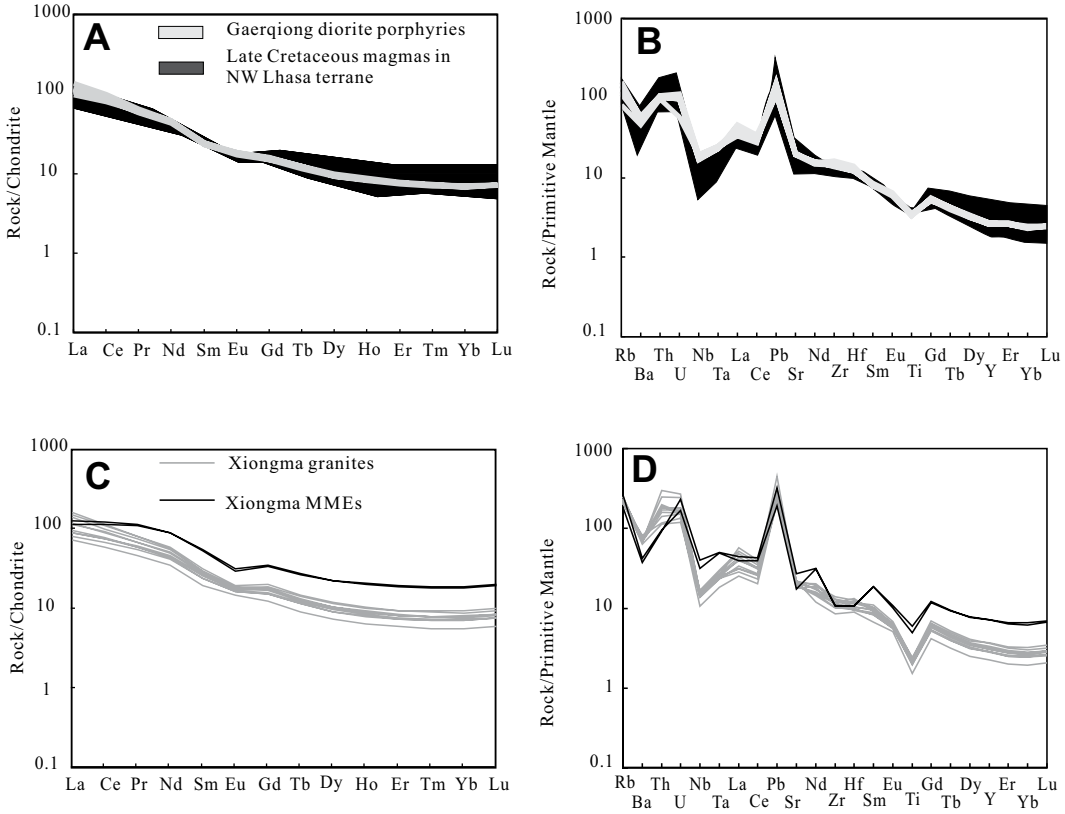

Figure 5. (A, B) Chondrite-normalized rare earth element (REE) and primitive-mantle-normalized trace-element patterns for the Gaerqiong diorite porphyries. (C, D) Chondrite-normalized REE and primitive-mantle-normalized trace-element patterns for the Xiongma plutons. Normalizing values are from Sun and McDonough (1989). Data sources are as follows: Late Cretaceous igneous rocks are from Qu et al. (2006), Xin et al. (2007), Zhao et al. (2008), Yu et al. (2011), Chen et al. (2015), Liu et al. (2015), Sun et al. (2015b), and Yi et al. (2018). MME—microgranular enclave.

magmatic textures (Figs. 2E and 2F). The lack of metamorphic textures, such as metacrystal texture (Didier and Barbarin, 1991), suggests that the Xiongma MMEs are not residual materials (restites) (e.g., Chappell et al., 1987; Chappell and White, 1991). The compositional gap between the Xiongma MMEs and the host granites indicates that the former cannot be the accumulations of the latter. The igneous microtextures and acicular apatites in the Xiongma MMEs, which are commonly observed in co-mingled mafic pillow lavas due to rapid cooling (Vernon and Williams, 1988), are usually the result of mingling between small volumes of hot basaltic melt and a cool granitic melt (Sparks and Marshall, 1986). Furthermore, the presence of K-feldspar megacrysts in the Xiongma MMEs also implies that they are remnants of a mafic component added to a silicic magma chamber (e.g., Troll and Schmincke, 2002).

Although petrographic observation confirms that the Xiongma MMEs show no alteration, one sample of Xiongma MMEs has a slightly high loss on ignition (LOI) value (3.8%), which might experience slight alteration. It's generally believed that alteration can affect concentrations of some mobile elements (e.g., Rb, Sr, and Ba). In contrast, elements such as rare earth elements (REEs) and high field strength elements (HFSEs) are not significantly affected by metamorphic processes (Hastie et al., 2007). We therefore mainly focus on REEs, HFSEs, and zircon Hf isotopic compositions in the following discussion about the petrogenesis of Xiongma MMEs. The Xiongma MMEs have relatively low SiO_2, but high MgO, Fe_2O_3, TiO_2, and Cr concentrations (Figs. 7A–7C; Table 1). Meanwhile, they are enriched in LREEs, depleted in HFSEs in primitive-mantle-normalized trace element patterns (Figs. 5C and 5D), and have negative $\varepsilon Hf_{(t)}$ isotopic compositions (–14.0 to –5.8). These geochemical features indicate that the MMEs were derived from either the lithospheric mantle enriched by recycled crustal materials or depleted asthenospheric mantle with significant crustal contamination. Asthenospheric-mantle-derived magmas affected by crustal contamination might produce mafic rocks with positive Zr-Hf anomalies due to the enrichment of these elements in crustal material (Rudnick and Gao, 2003). However, the Xiongma MMEs do not display positive Zr-Hf anomalies in primitive-mantle-normalized trace-element patterns (Fig. 5D). The Xiongma MMEs have trace-element patterns and enriched isotopic compositions similar to the Early Cretaceous (110 Ma) Nixiong dioritic enclaves ($\varepsilon Hf_{(t)}$ values of –14 to –0.2) in the Coqen area, which were formed by melting of heterogeneous lithospheric mantle (Zhang, 2012). We therefore propose that the Xiongma MMEs were produced by partial melting of enriched lithospheric mantle.

Petrogenesis of the Host Granites

The Xiongma granites are metaluminous to weakly peraluminous and contain amphibole rather than typical peraluminous minerals. Meanwhile, their P_2O_5 content decreases with increasing SiO_2 (Supplementary Fig. DR1; see footnote 1). Futhermore, they have low zircon saturation temperatures (~769 °C; Watson and Harrison, 1983, Table 1). These geochemical characteristics show that the Xiongma granites are I-type granites (Chappell and White, 1992). I-type granites are usually formed in three ways: (1) FC of basaltic melts (White and Chappell, 1977); (2) partial melting of the lower continental crust (Chappell and White, 2001); and (3) mixing of crust- and mantle-derived melts (Janoušek et al., 2004).

It is generally accepted that I-type granites can be produced by the FC of mafic magmas (White and Chappell, 1977; Soesoo, 2000). The contemporaneous mafic rocks were reported in the Coqen area (Qu et al., 2006), and it is possible that the Xiongma granites could have been formed by the FC of mafic magmas. However, this hypothesis is inconsistent with the following lines of evidence: (1) significant compositional gaps exist between the Xiongma granites and the mafic rocks; (2) the trace element ratios of the Xiongma granites, such as Cr/Th (0.30–1.84) and Sr/Ba (0.74–0.96), are different from those of the mafic rocks (Cr/Th = 26.4; Sr/Ba = 1.38);

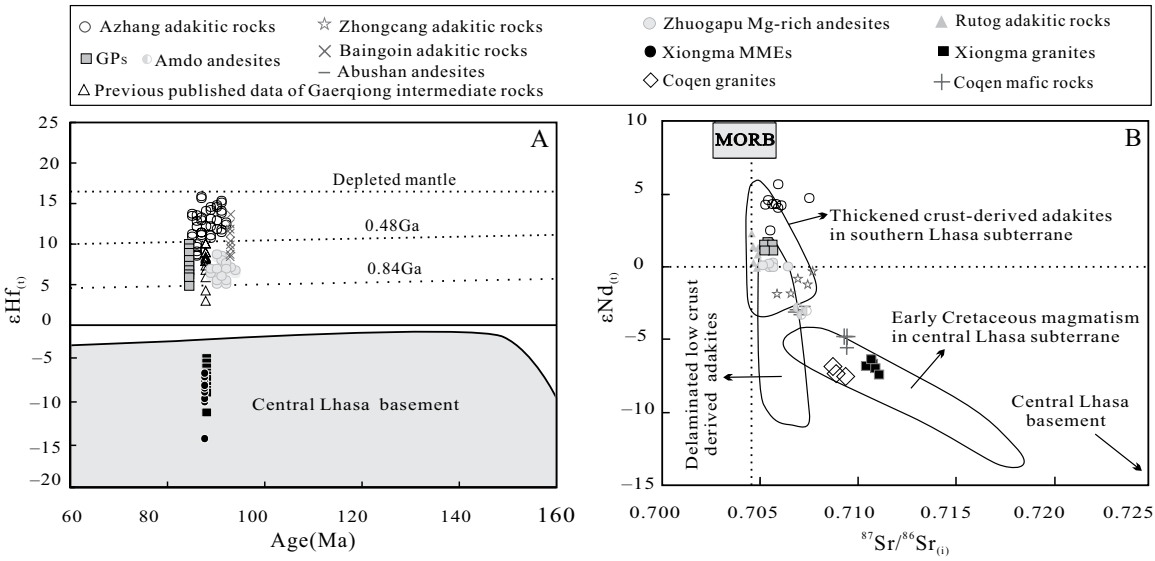

Figure 6. (A) $\varepsilon Hf_{(t)}$ versus U-Pb zircon age diagram. (B) $^{87}Sr/^{86}Sr_{(i)}$ versus $\varepsilon Nd_{(t)}$ diagram. Data sources are as follows: central Lhasa basement are from Zhu et al. (2009, 2011); MORB (mid-oceanic ridge basalt) of the Bangonghu-Nujiang Suture Zone are from Qiu et al. (2007); Miocene adakitic rocks of the southern Lhasa subterrane are from Hou et al. (2004); adakitic rocks derived from delaminated lower crust are from Xu et al. (2002) and Gao et al. (2004); Early Cretaceous rocks within the central Lhasa subterrane are from Zhou et al. (2008) and Zhu et al. (2009, 2011); other data sources are as in Fig. 4. GPs—Gaerqiong diorite porphyries.

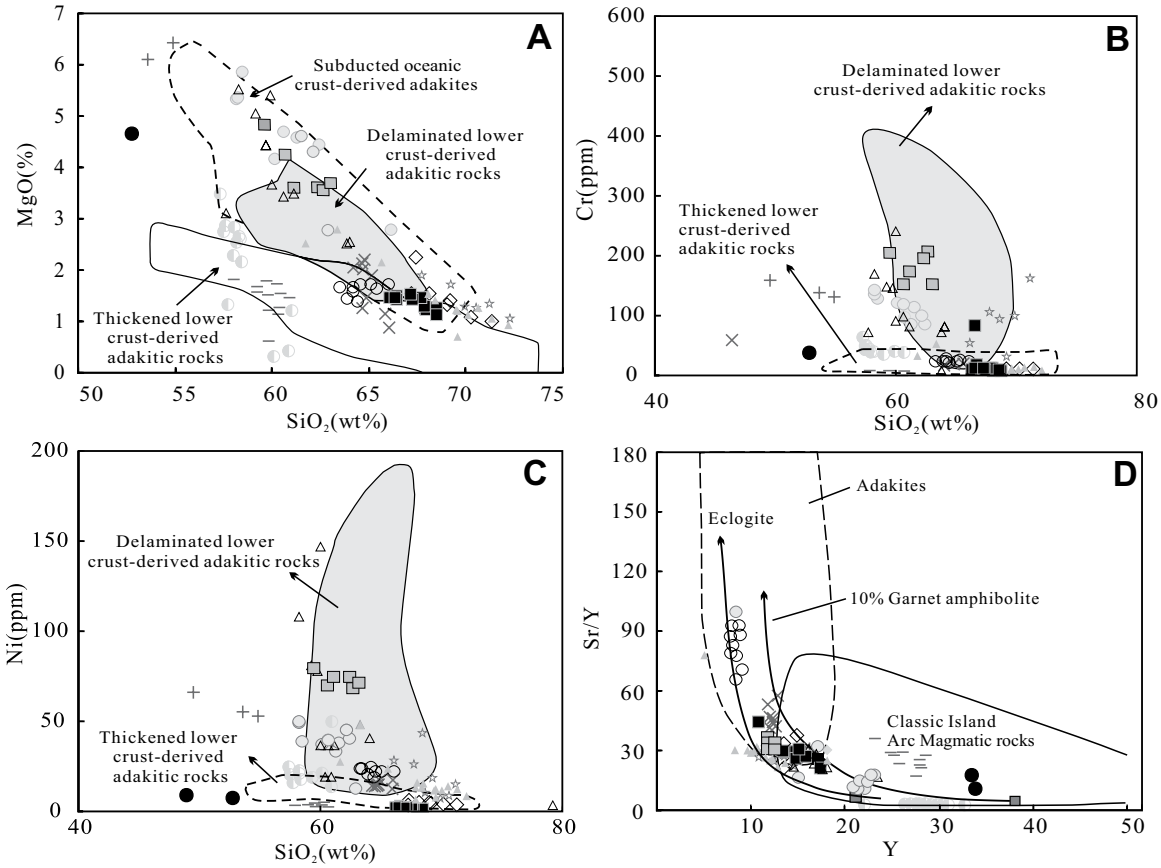

Figure 7. Diagrams of (A) SiO_2 versus MgO, (B) SiO_2 versus Cr, (C) SiO_2 versus Ni, and (D) Sr/Y versus Y (after Defant and Drummond, 1990). The fields for delaminated lower crust, subducted oceanic crust, and thickened lower continental crust are from the compilations of Wang et al. (2006) and Chen et al. (2013). Data sources and symbols are as in Fig. 4.

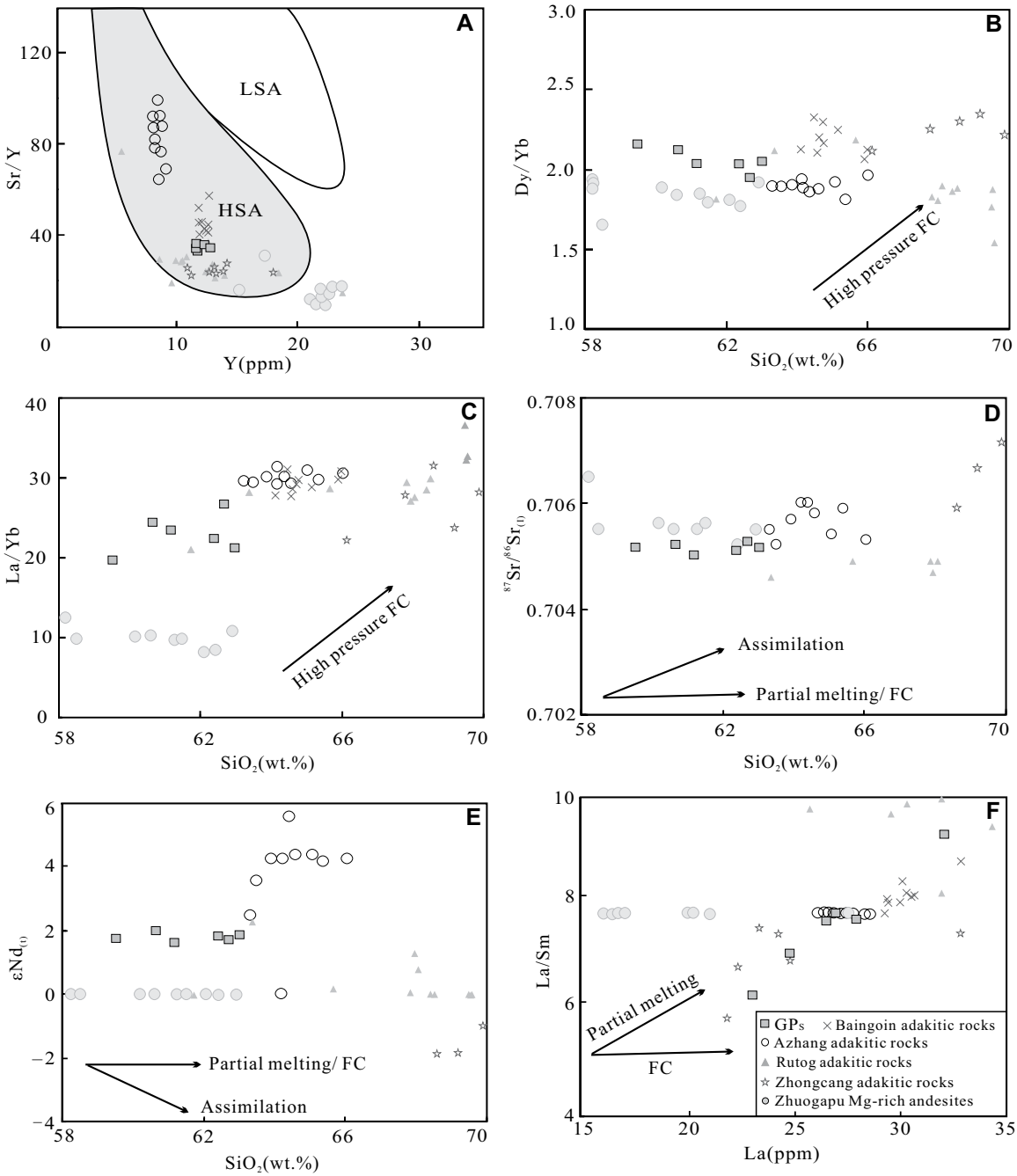

Figure 8. Diagrams of (A) Sr/Y versus Y (the fields for low-SiO_2 [LSA] and high-SiO_2 [HSA] adakites are from Martin et al., 2005), (B) SiO_2 versus Dy/Yb, (C) SiO_2 versus La/Yb, (D) SiO_2 versus $^{87}Sr/^{86}Sr_i$, (E) SiO_2 versus $\varepsilon Nd_{(t)}$, and (F) La versus La/Sm. Data sources are as in Fig. 4. FC—fractional crystallization.

and (3) the volumes of the Xiongma granites are larger than those of the mafic rocks in the studied area. Thus, the Xiongma granites were not generated solely by the FC of mafic magmas.

The metaluminous Xiongma granites have relatively high SiO_2 and low MgO contents, suggesting that their parental magmas were derived from a crustal source (Rudnick, 1995). As the Xiongma granites are exposed in the central Lhasa subterrane (a microcontinent with Precambrian basement; Allègre et al., 1984), they should have negative whole-rock $\varepsilon Nd_{(t)}$ and zircon $\varepsilon Hf_{(t)}$ values, similar to the ancient central Lhasa subterrane ($\varepsilon Nd_{(t)} = -15.4$; $\varepsilon Hf_{(t)} = -17.3$ to -2.5; Zhu et al., 2011). However, the Xiongma granites have much higher whole-rock $\varepsilon Nd_{(t)}$ (-7.4 to -6.3) and zircon $\varepsilon Hf_{(t)}$ (-11.0 to -4.1) values than those values of the central Lhasa subterrane (Figs. 6A and 6B). Thus, the formation of the Xiongma granites cannot be attributed to simple partial melting of the lower crust of the ancient central Lhasa subterrane.

The Xiongma granites have the Sr-Nd isotopic values similar to those of the Coqen granites, which were proposed to be formed by mixing of crust-derived magmas and enriched-mantle-derived magmas (Qu et al., 2006, Xin

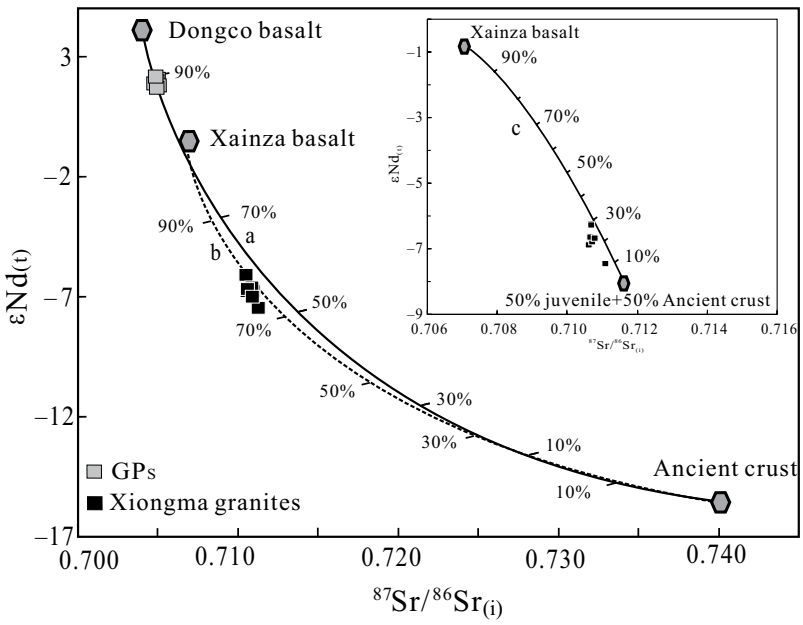

Figure 9. $^{87}Sr/^{86}Sr_{(i)}$ versus $\varepsilon Nd_{(t)}$ diagram for the Gaerqiong diorite porphyries (GPs) and the host Xiongma granites. The compositions of end-members used for the GPs are as follows: depleted-mantle-derived magmas (represented by Dongco basalt sample 11DC-27; Wang et al., 2016a) with $^{87}Sr/^{86}Sr_{(i)}$ = 0.7043, $\varepsilon Nd_{(t)}$ = 41.4, Sr = 571 ppm, and Nd = 41.4 ppm; Lhasa basement-derived magmas (represented by strongly peraluminous granite sample 08DX17; Zhu et al., 2011) with $^{87}Sr/^{86}Sr_{(i)}$ = 0.7402, $\varepsilon Nd_{(t)}$ = –15.4, Sr = 131 ppm, and Nd = 43.4 ppm. The compositions of end-members used for the Xiongma host granites are as follows: enriched-mantle-derived magmas (represented by Xainza basalt sample SZ12-2; Chen et al., 2014) with $^{87}Sr/^{86}Sr_{(i)}$ = 0.7070, $\varepsilon Nd_{(t)}$ = –0.9, Sr = 262 ppm, and Nd = 19.7 ppm; Lhasa basement-derived magmas (represented by strongly peraluminous granite sample 08DX17; Zhu et al., 2011) with $^{87}Sr/^{86}Sr_{(i)}$ = 0.7402, $\varepsilon Nd_{(t)}$ = –15.4, Sr = 131 ppm, and Nd = 43.4 ppm; and the juvenile crust-derived magmas (represented by Azhang adakite sample LS-N; Sun et al., 2015b) with $^{87}Sr/^{86}Sr_{(i)}$ = 0.7060, $\varepsilon Nd_{(t)}$ = 5.6, Sr = 668 ppm, and Nd = 23.3 ppm. The mixing curve "a" is for the GPs, while "b" and "c" are for the Xiongma granites.

et al., 2007). Meanwhile, the widely variable zircon $\varepsilon Hf_{(t)}$ values (Fig. 6A) of the Xiongma granites, together with the presence of MMEs and the relationship between 1/Sr and $^{87}Sr/^{86}Sr_{(i)}$ values (Supplementary Fig. DR2; see footnote 1), indicate that Xiongma granites were resulted from mixing between crust-derived magmas and enriched-mantle-derived magmas. To test whether Xiongma granites can be formed by the two magmas mixing, we employ a simple isotopic modeling assuming that the enriched-mantle-derived basaltic end-member was represented by the Xainza basalt ($^{87}Sr/^{86}Sr_{(i)}$ = 0.7070, $\varepsilon Nd_{(t)}$ = –0.9, Chen et al., 2014) from the northern Lhasa subterrane; and ancient crust-derived felsic end-member was represented by the strongly peraluminous S-type granite ($^{87}Sr/^{86}Sr_{(i)}$ = 0.7402, $\varepsilon Nd_{(t)}$ = –15.4, Zhu et al., 2011) from the central Lhasa subterrane. The geochemical modeling shows that the Xiongma host granites can be generated by mixing between 30% ancient crust-derived magmas and 70% enriched-mantle-derived magmas (Fig. 9). However, mixing of granitic magmas with such large volumes of mafic magmas does not account for the higher SiO_2 contents of the Xiongma granites. Therefore, juvenile crust (represented by the source of the Azhang adakite) beneath the central Lhasa subterrane (Sun et al., 2015b; this study) may have supplied material involved in the formation of the Xiongma granites. This view is consistent with the geochemical modeling result that the Xiongma granites can be formed by the mixing of 78% crust-derived magmas (comprising 50% ancient and 50% juvenile crust) and 22% enriched-mantle-derived magmas (Fig. 9).

Based on the petrography, major- and trace-element data, and Sr-Nd-Hf isotopic data for the MMEs and their host granites, a complex process is proposed for the formation of the XPs as follows. The host granites were the result of mixing of (ancient and juvenile) crust-derived magmas and enriched-mantle-derived magmas beneath the central Lhasa subterrane. In contrast, the MMEs were derived mainly from an enriched mantle source that incorporated crustal material through magma mixing.

Juvenile Crust beneath the Ancient Central Lhasa Subterrane

Zircon $\varepsilon Hf_{(t)}$ isotopic compositions have been used to divide the Lhasa terrane into the southern, central, and northern Lhasa subterranes (Zhu et al., 2011, 2013). Compared with the positive $\varepsilon Hf_{(t)}$ isotopic values of the southern and northern Lhasa subterranes, the negative $\varepsilon Hf_{(t)}$ values of the central Lhasa subterrane suggest it contains ancient basement (Zhu et al., 2011, 2013). As mentioned before, the formation of the GPs and XPs in central Lhasa subterrane required contributions from juvenile crustal materials. A similar conclusion was reached by Sun et al. (2015b), who suggested that the Azhang adakitic rocks with highly depleted $\varepsilon Hf_{(t)}$ in the central Lhasa subterrane were produced by partial melting of the juvenile mafic lower crust. An intriguing question is why and when this juvenile crust existed in the central Lhasa subterrane, given that it was proved to be the ancient basement (Zhu et al., 2009, 2011, 2013).

Recent studies have shown that the Xainza and Yanhu basalts (ca. 113 Ma) have geochemical characteristics similar to those of within-plate basalts, in contrast to the Early Cretaceous (ca. 140–120 Ma) arc-like basalts of the Duoni and Qushenla formations in the NW Lhasa Terrane (Kang et al., 2009, 2010; Sui et al., 2013; Chen et al., 2014). It was suggested that the underplating of mantle-derived mafic magmas beneath the NW Lhasa Terrane might provide material for the formation of the Xainza and Yanhu within-plate basalts (Sui et al., 2013; Chen et al., 2014). This mafic magmas underplating event may have occurred in response to slab roll-back and break-off of the southward-subducting Bangong-Nujiang oceanic lithosphere during the Early Cretaceous (Zhu et al., 2009, 2011, 2013). The recently discovered Early Cretaceous granodiorites and granite porphyries with depleted isotopic compositions ($\varepsilon Nd_{(t)}$ = +1.4 to +2.7) in the Gerze area also indicate that the mafic magmas underplating event occurred beneath the NW Lhasa Terrane (Dong et al., 2016). Therefore, the juvenile crust beneath the ancient central Lhasa subterrane was likely formed during the Early Cretaceous due to this mafic magmas underplating event.

TECTONIC IMPLICATIONS

Tectonic Evolution of the NW Lhasa Terrane

Whether the geodynamic mechanism corresponding to the Late Cretaceous magmatic activity in the NW Lhasa Terrane (Supplemen-

tary Table DR2; see footnote 1) was in a subduction setting related to the evolution of the Neo-Tethys (Indus–Yarlung Zangbo) or a post-collisional extensional setting linked to the evolution of Bangong-Nujiang oceans was in a hot debate (Qu et al., 2006; Xin et al., 2007; Zhao et al., 2008; Ma and Yue, 2010; Yu et al., 2011; Wang et al., 2014; Chen et al., 2015; Sun et al., 2015b;Yi et al., 2018).

Ma et al. (2015) suggested that the Late Cretaceous (ca. 90 Ma) igneous rocks within the central Lhasa subterrane can be formed by slab roll-back of the Neo-Tethys. However, based on the following lines of evidence, we suggest that the Late Cretaceous (ca. 90 Ma) magmatic rocks in NW Lhasa Terrane were unlikely in a back-arc setting related to slab roll-back of the Neo-Tethys. Firstly, slab roll-back of the Neo-Tethys in the Late Cretaceous was based on the assumption that subduction of the Neo-Tethyan oceanic lithosphere occurred at a flat/low-angle during the Early Cretaceous (140–110 Ma), which was proposed to explain the scarcity of Early Cretaceous igneous rocks in the southern Lhasa subterrane (Coulon et al., 1986; Kapp et al., 2007). However, recent studies have identified Early Cretaceous magmatic rocks in the southern and central Lhasa subterrane, which is inconsistent with this assumption (Ji et al., 2009; Wu et al., 2010; Zhu et al., 2011). Meanwhile, the results of a sedimentological study by Sun et al. (2015a) suggest that the Coqen Basin was a local foreland basin linked to the south-directed contraction of the northern Lhasa subterrane, rather than a back-arc extensional basin related to slab roll-back of the Neo-Tethys during the Late Cretaceous. Furthermore, the mafic dikes in the Coqen area have high Zr concentrations (115 ppm) and Zr/Y ratios (>7; Qu et al., 2006), and therefore resemble within-plate basalts rather than back-arc basin basalts (e.g., X.C. Wang et al., 2016b). Thus, the Late Cretaceous magmatic rocks in the NW Lhasa Terrane were unlikely controlled by the Neo-Tethys subduction, although the effect of Neo-Tethys subduction on this region cannot be totally excluded.

Alternatively, the Late Cretaceous magmatic activity in the NW Lhasa Terrane can be linked to the evolution of the Bangong-Nujiang Ocean (Qu et al., 2006; Xin et al., 2007; Yu et al., 2011; Wang et al., 2014; Chen et al., 2015; Sun et al., 2015b; Yi et al., 2018). Recently, the discovery of the Early Jurassic Gajia mélange in the Bangong-Nujiang suture zone proves that the southward subduction of the Bangong-Nujiang slab had already occurred during the Early Jurassic (Lai et al., 2017). In addition, previous researches indicated that the Jurassic–Early Cretaceous magmatic rocks in the NW Lhasa Terrane recorded the evolution of Bangong-Nujiang Tethys, i.e., the Jurassic–Early Cretaceous southward subduction and the Early Cretaceous continental syn-collisional setting (Zhu et al., 2009, 2011, 2013; S.S. Chen et al., 2017a). More importantly, the following lines of evidence indicate that the Late Cretaceous magmatic activity in the NW Lhasa Terrane occurred into a post-collisional extensional setting after collision of the Lhasa-Qiangtang Terranes. Firstly, compared with the narrow belt of the syn-collisional Early Cretaceous magmatic rocks (143–110 Ma) in the NW Lhasa Terrane, the Late Cretaceous magmatic rocks (ca. 90 Ma) in this region were distributed more sparsely, consistent with the distribution of the post-subduction ("post-orogenic") magmatism (Fig. 1B; S.S. Chen et al., 2017a). Secondly, the widely distributed Jingzhushan Formation (100–93 Ma) in the NW Lhasa Terrane (Li, 2008) unconformably overlies the Langshan marine limestone, which was thought to mark the transition from an oceanic subduction system to an intraplate tectonic system (Kapp et al., 2007; Li, 2008). Thirdly, bimodal volcanic rocks, mafic dikes, and intracontinental high-$Mg^{\#}$ adakitic rocks were reported in the studied region, which are usually developed in a post-collisional extensional setting (Xin et al., 2007; Yu et al., 2011; Zhang et al., 2014; Chen et al., 2015; Yi et al., 2018; this study). Finally, the Early Cretaceous tectonic deformation in the NW Lhasa Terrane was dominant ~E-W–striking schistosity and thrust faults, indicating ~N-S compression (Kapp et al., 2005, 2007; Li, 2014). In contrast, the Late Cretaceous deformation was characterized by ~E-W–striking normal and detachment faults, indicating ~N-S extension (Li, 2014). Therefore, the NW Lhasa Terrane probably entered into a post-collisional extensional phase during the Late Cretaceous (Wang et al., 2014; Chen et al., 2015; Sun et al., 2015b; Yi et al., 2018).

The geodynamic models including the continental crustal delamination and slab break-off have been proposed for the formation of the Late Cretaceous magmatic rocks in the NW Lhasa Terrane (Yu et al., 2011; Wang et al., 2014; Chen et al., 2015; Lei et al., 2015; Sun et al., 2015b; Li et al., 2017; Yi et al., 2018). Nonetheless, the following observations do not support the slab break-off model. Firstly, the ca. 110 Ma magmatic "flare-up" event in the NW Lhasa Terrane (involving significant input of mantle-derived materials) has been attributed to break-off of the southward-subducting Bangong-Nujiang oceanic slab (Sui et al., 2013; Chen et al., 2014). This corresponds well with the results of thermo-mechanical modeling, which indicates that slab break-off occurs mostly within 15–20 m.y. after continental collision (ca. 140–125 Ma) (Macera et al., 2008; van Hunen and Allen, 2011). Thus, break-off of the southward-subducting Bangong-Nujiang oceanic slab probably occurred at ca. 110 Ma, rather than at ca. 90 Ma (Zhu et al., 2011; Sui et al., 2013; Chen et al., 2014). Secondly, slab break-off typically results in the formation of a relatively narrow and linear zone of magmatism along the suture (e.g., Kohn and Parkinson, 2002; Mahéo et al., 2002), in contrast to the sporadic distribution of the Late Cretaceous magmatic rocks in the NW Lhasa Terrane (Fig. 1B). Thirdly, intracontinental high-$Mg^{\#}$ adakitic rocks were found in this area, which are typically associated with lithospheric delamination (Xu et al., 2002; Gao et al., 2004; Wang et al., 2006). The lithospheric delamination model is, therefore, the more suitable geodynamic mechanism to explain the formation of the Late Cretaceous magmatic rocks in the NW Lhasa terrane.

In summary, following the southward subduction of the Bangong-Nujiang oceanic slab and collision of the Qiangtang-Lhasa terranes, the NW Lhasa Terrane entered a post-collisional extensional setting during the Late Cretaceous (ca. 90 Ma). This extensional setting was related to regional lithospheric delamination at Late Cretaceous (ca. 90 Ma), which triggered episodic magmatism in the NW Lhasa Terrane.

Implications for Uplift of the Tibetan Plateau

Previous studies attributed the crustal thickening and uplift of the Tibetan Plateau primarily to India-Asia continental collision during the Cenozoic (e.g., Turner et al., 1993, 1996; Chung et al., 1998, 2005). However, the following observations show that the lower crust of NW Lhasa terrane has been thickened since the late Mesozoic. (1) The early Late Cretaceous (100–93 Ma) foreland molasses (widespread in the NW Lhasa Terrane) usually mark the end of orogenic movement (Li, 2008). (2) An inferred high mountain range had been developed in the NW Lhasa terrane, which provided sediments to the Coqen Basin during the Late Cretaceous (Sun et al., 2015a). (3) The transition from marine to nonmarine facies in the Nyima region commenced at ca. 120–110 Ma in the NW Lhasa Terrane, together with major upper-crustal shortening (Kapp et al., 2007). (4) Detailed study of the deposition of the Damxung Conglomerate revealed a phase of significant topographic growth and crustal thickening of the NW Lhasa Terrane at ca. 110 Ma (Wang et al., 2017).

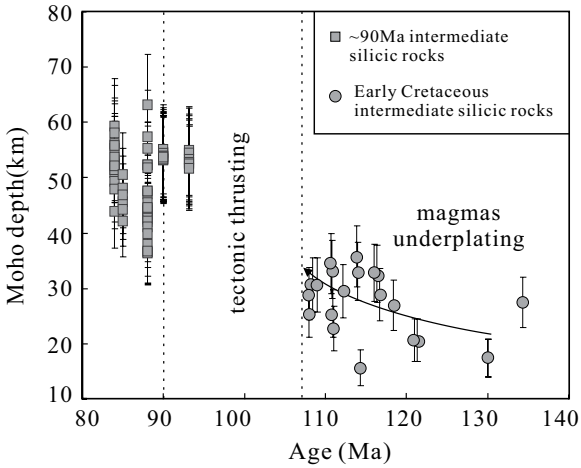

Figure 10. Plot of Moho depth versus age for Late Cretaceous (ca. 90 Ma) and Early Cretaceous intermediate-silicic rocks of the NW Lhasa Terrane. The empirical relationship between La/Yb values and crustal thickness ($(La/Yb)_N = 2.94e^{(0.036D_M)}$, or $D_M = 27.78\ln[0.34(La/Yb)_N]$, where $(La/Yb)_N$ is whole-rock value, and D_M is crustal thickness or Moho depth) from Hu et al. (2017) is used to track the crustal thickness of the NW Lhasa Terrane. Data sources are as follows: Late Cretaceous (ca. 90 Ma) intermediate-silicic rocks are from Qu et al. (2006), Xin et al. (2007), Zhao et al. (2008), Yu et al. (2011), Chen et al. (2015), Liu et al. (2015), Sun et al. (2015b), Yi et al. (2018), and this study; Early Cretaceous rocks are from Zhou et al. (2008) and Zhu et al. (2009, 2011).

The Cretaceous continental intermediate-silicic rocks in the NW Lhasa Terrane can provide additional constraints on the surface elevation of the region. Compared with the Early Cretaceous intermediate-silicic rocks, most of the Late Cretaceous rocks show adakitic affinities, indicating that they originated from the thickened lower crust in the stability field of garnet and/or amphibole (corresponding to crustal depths of 50 km; Zhao et al., 2008; Chen et al., 2015; Sun et al., 2015b; Yi et al., 2018; this study). The Sr/Y and La/Yb ratios of intermediate-silicic igneous rocks in subduction-related arcs correlate well with crustal thickness at global and regional scales (Chapman et al., 2015; Profeta et al., 2015). However, whether this correlation can be applied to continental collisional orogens has yet to be tested (Profeta et al., 2015). Hu et al. (2017) compiled major- and trace-element data of Miocene and younger intrusive and extrusive rocks from six continental collisional orogens (including Southern Tibet) and established empirical relationships between geochemical indices and crustal thickness or Moho depth ($(La/Yb)_N = 2.94e^{(0.036D_M)}$, or $D_M = 27.78\ln[0.34(La/Yb)_N]$, where $(La/Yb)_N$ is whole-rock value, and D_M is crustal thickness or Moho depth) by performing a least-squares regression of the collected data. The empirical relationship between the La/Yb ratios of global intermediate-silicic rocks and crustal thickness, as reported by Hu et al. (2017), is used to track the changes in Cretaceous crustal thickness of the NW Lhasa Terrane, as this approach is most suitable for continental collisional orogens (Supplementary Text DR2; see footnote 1). The $(La/Yb)_N$ values complied here indicate that the crustal thickness of the NW Lhasa Terrane began to increase at a slow rate and ultimately reached a normal thickness of ~35 km (Fig. 10). This period of crustal thickening is attributed to mafic underplating related to slab roll-back and break-off of the southward-subducting Bangong-Nujiang oceanic lithosphere during the Early Cretaceous (140–113 Ma; Sui et al., 2013; Chen et al., 2014). This hypothesis is consistent with the conclusions of recent studies, which emphasize the role of magmas underplating in crustal thickening and surface uplift (Lee et al., 2015; Perkins et al., 2016; Chen et al., 2018). Compared with the Early Cretaceous crustal thickness of the NW Lhasa Terrane, the Late Cretaceous (ca. 90 Ma) crustal thickness increased to an average thickness of ~50 km (Fig. 10). This empirical result is consistent with the fact that the central Tibetan Plateau (comprising the Lhasa and Qiangtang terranes) experienced moderate to rapid exhumation during the Late Cretaceous, as revealed by low-temperature thermochronology (Hetzel et al., 2011; Rohrmann et al., 2012). This period of abrupt change in crustal thickening was most likely related to tectonic thrusting caused by collision between the Lhasa and Qiangtang terranes during the late Early Cretaceous (110–90 Ma; Rohrmann et al., 2012). The ~20 m.y. period of contraction may have been sufficient to generate a deformable and thickened lithospheric root below the NW Lhasa Terrane before the Late Cretaceous (ca. 90 Ma) (e.g., Lustrino, 2005). Given that the lowermost crust of the NW Lhasa Terrane had already been delaminated during the Late Cretaceous (ca. 90 Ma), the maximum crustal thickness (average of >50 km) of this region would have been attained before this time. However, due to the presence of magmatic lull at 107–90 Ma in the NW Lhasa Terrane (Zhu et al., 2009), the exact time when the crust of NW Lhasa terrane reached its maximum thickness is unclear and requires further study to know.

It should be noted that the intermediate-silicic rocks from the northern part of the NW Lhasa terrane have obvious adakitic affinities with no negative Eu anomalies (e.g., GPs, Rutog, Azhang, and Zhongcang adakitic rocks), indicating that these rocks were generated by partial melting of (garnet amphibolite) eclogites. In contrast, the Xiongma granites from the central part of the NW Lhasa terrane have low Y contents and negative Eu anomalies, without an adakitic affinity (Fig. 7D; Table 1), indicating that they were most likely generated by partial melting of the source with garnet and plagioclase as residual minerals (Rapp and Watson, 1995). This implies that the crust of the central part of the NW Lhasa terrane was less thickened than the northern part. This hypothesis is consistent with the increasing La/Yb values of the intermediate-silicic rocks from the central to northern parts of the terrane as above description (Fig. 11). This variable crustal thickness in this terrane can be explained by the following reasons: (1) the thickened eclogitic lower crust of the central area had already been delaminated into the mantle, or (2) the central area was far from the BNSZ and therefore the effects of crustal/lithospheric shortening and magmatic underplating were less intense than the northern, resulting in less crustal thickening.

In summary, we propose that magmatic underplating and subsequent tectonic thrusting may have caused crustal thickening of the NW Lhasa Terrane since the Cretaceous, and the crust reached its maximum thickness (average of >50 km) before the Late Cretaceous (ca. 90 Ma). Given that crustal thickening generally results in elevated terrain, the uplift of the NW Lhasa Terrane (driven by isostasy due to crustal thickening) probably commenced before the Late Cretaceous (ca. 90 Ma).

CONCLUSIONS

The new geochronology, geochemical, and Sr-Nd-Hf isotopic values of two plutons (GPs and XPs), combined with previous research, show that an important magmatic event occurred within the NW Lhasa Terrane during the Late Cretaceous. The Late Cretaceous (ca. 90 Ma) magmatic activity occurred in a post-collisional extensional setting and was triggered by regional lithospheric delamination after the collision of the Lhasa-Qiangtang

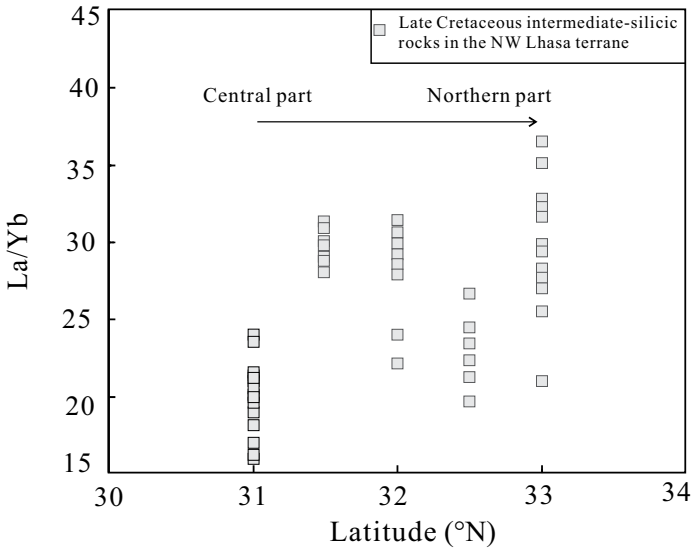

Figure 11. La/Yb values of Late Cretaceous (ca. 90 Ma) intermediate-silicic rocks of the NW Lhasa Terrane plotted against latitude. Data sources are as follows: intermediate-silicic rocks in the central part of the NW Lhasa Terrane are from Qu et al. (2006), Xin et al. (2007), and this study; intermediate-silicic rocks in the northern part of the NW Lhasa Terrane are from Zhao et al. (2008), Yu et al. (2011), Chen et al. (2015), Liu et al. (2015), Sun et al. (2015b), Yi et al. (2018), and this study.

Terranes. This indicates that the NW Lhasa Terrane was characterized by a thickened continental crust prior to the Late Cretaceous (ca. 90 Ma). The thickened crust in this area may have been related to basaltic magma underplating and tectonic thrusting. The magma underplating was triggered by slab roll-back and break-off of the southward-subducting Bangong-Nujiang oceanic lithosphere during the Early Cretaceous (140–113 Ma), whereas tectonic thrusting was caused by collision of the Lhasa and Qiangtang Terranes in the late Early–early Late Cretaceous (110–90 Ma). The crust of the NW Lhasa Terrane reached its maximum average thickness (average of >50 km) before the Late Cretaceous (ca. 90 Ma), indicating that uplift of the terrane commenced prior to this time.

ACKNOWLEDGMENTS

We are grateful to the science editor, Professor B.S. Singer, associate editor, Professor H.B. Zou, three anonymous reviewers and Dr. S.S. Chen for their constructive reviews and suggestions. We would like to thank Guangqian Hu, Xirong Liang, Xiangling Tu, Ying Liu, and Le Zhang for their assistance with laboratory. This study was financially supported by the Chinese National Key Research and Development Program (2016YFC0600305), Chinese Major State Basic Research Program (2015CB452602), Chinese National Science Foundation (41573024, 41873037), and the GIGCAS 135 project (135TP201601). This is contribution No. IS-2655 of GIGCAS.

REFERENCES CITED

Allègre, C. J., Courtillot, V., Tapponnier, P., Hirn, A., Mattauer, M., Coulon, C., Jaeger, J. J., Achache, J., Schaerer, U., Marcoux, J., Burg, J. P., Girardeau, J., Armijo, R., Gariepy, C., Goepel, C., Tindong, L., Xuchang, X., Chenfa, C., Guanggin, L., Baoyu, L., Wen, T. J., Naiwen, W., Guoming, C., Tonglin, H., Xibin, W., Wanming, D., Huaibin, S.,Yougong, C., Ji, Z., Hongrong, Q., Peisheng, B., Songchan, W., Bixiang, W.,Yaoxiu, Z., and Xu, R., 1984, Structure and evolution of the Himalaya-Tibet orogenic belt: Nature, v. 307, p. 17–22, https://doi.org/10.1038/307017a0.

Andersen, T., 2002, Correction of common lead in U–Pb analyses that do not report ^{204}Pb: Chemical geology, v. 192, p. 59–79, https://doi.org/10.1016/S0009-2541(02)00195-X.

Bonin, B., 1991, The enclaves of alkaline anorogenic granites: an overview, *in* Didier, J., and Barbarin, B., eds., Enclaves and Granite Petrology, Developments in Petrology: Amsterdam, Elsevier, v. 13, p. 179–189.

Castillo, P.R., Janney, P.E., and Solidum, R.U., 1999, Petrology and geochemistry of Camiguin island, southern Philippines: Insights to the source of adakites and other lavas in a complex arc setting: Contributions to Mineralogy and Petrology, v. 134, p. 33–51, https://doi.org/10.1007/s004100050467.

Chapman, J.B., Ducea, M.N., DeCelles, P.G., and Profeta, L., 2015, Tracking changes in crustal thickness during orogenic evolution with Sr/Y: An example from the North American Cordillera: Geology, v. 43, p. 919–922, https://doi.org/10.1130/G36996.1.

Chappell, B.W., White, A.J.R., and Wyborn, D., 1987, The importance of residual source material (restite) in granite petrogenesis: Journal of Petrology, v. 28, p. 1111–1138, https://doi.org/10.1093/petrology/28.6.1111.

Chappell, B.W., and White, A.J.R., 1991, Restite enclaves and the restite model, *in* Didier, J., and Barbarin, B., eds., Developments in Petrology: Amsterdam, Elsevier, v. 13, p. 375–381.

Chappell, B.W., and White, A.J.R., 1992, I- and S-type granites in the Lachlan Fold Belt: Transactions of the Royal Society of Edinburgh: Earth and Environmental Science, v. 83, p.1–26, https://doi.org/10.1017/S0263593300007720.

Chappell, B.W., and White, A.J.R., 2001, Two contrasting granite types: 25 years later: Australian Journal of Earth Sciences, v. 48, p. 489–499, https://doi.org/10.1046/j.1440-0952.2001.00882.x.

Chen, J.L., Xu, J.F., Wang, B.D., Kang, Z.Q., and Li, J., 2010, Origin of Cenozoic alkaline potassic volcanic rocks at KonglongXiang, Lhasa terrane, Tibetan Plateau: Products of partial melting of a mafic lower-crustal source: Chemical Geology, v. 273, p. 286–299, https://doi.org/10.1016/j.chemgeo.2010.03.003.

Chen, J.L., Wu, J.B., Xu, J.F., Dong, Y.H., Wang, B.D., and Kang, Z.Q., 2013, Geochemistry of Eocene high-Mg# adakitic rocks in the northern Qiangtang terrane, central Tibet: Implications for early uplift of the plateau: Geological Society of America Bulletin, v. 125, p. 1800–1819, https://doi.org/10.1130/B30755.1.

Chen, J.L., Xu, J.F., Yu, H.X., Wang, B.D., Wu, J.B., and Feng, Y.X., 2015, Early late Cretaceous high-Mg# granitoids in southern Tibet: Implications for the early crustal thickening and tectonic evolution of the Tibetan Plateau: Lithos, v. 232, p. 12–22, https://doi.org/10.1016/j.lithos.2015.06.020.

Chen, J.L., Yin, A., Xu, J.F., Wang, B.D., Dong, Y.H., and Kang, Z.Q., 2018, Late Cenozoic magmatic inflation, crustal thickening, and >2 km of surface uplift in central Tibet: Geology, v. 46, p. 19–22, https://doi.org/10.1130/G39699.1.

Chen, S.S., Shi, R.D., Gong, X.H., Liu, D.L., Huang, Q.S., Yi, G.D., Wu, K., and Zou, H.B., 2017a, A syn-collisional model for Early Cretaceous magmatism in the northern and central Lhasa subterranes: Gondwana Research, v. 41, p. 93–109, https://doi.org/10.1016/j.gr.2015.04.008.

Chen, S.S., Fan, W.M., Shi, R.D., Gong, X.H., and Wu, K., 2017b, Removal of deep lithosphere in ancient continental collisional orogens: A case study from central Tibet, China: Geochemistry Geophysics Geosystems, v. 18, p. 1225–1243, https://doi.org/10.1002/2016GC006678.

Chen, Y., Zhu, D.C., Zhao, Z.D., Meng, F.Y., Wang, Q., Santosh, M., Wang, L.Q., Dong, G.C., and Mo, X.X., 2014, Slab breakoff triggered ca. 113Ma magmatism around Xainza area of the Lhasa Terrane, Tibet: Gondwana Research, v. 26, p. 449–463, https://doi.org/10.1016/j.gr.2013.06.005.

Chung, S., Lo, C., Lee, T., Zhang, Y., Xie, Y., Li, X., Wang, K., and Wang, P., 1998, Diachronous uplift of the Tibetan plateau starting 40 Myr ago: Nature, v. 394, p. 769–773, https://doi.org/10.1038 /29511.

Chung, S.L., Chu, M.F., Zhang, Y., Xie, Y., Lo, C.H., Lee, T.Y., Lan, C.Y., Li, X., Zhang, Q., and Wang, Y., 2005, Tibetan tectonic evolution inferred from spatial and temporal variations in post-collisional magmatism: Earth-Science Reviews, v. 68, p. 173–196, https://doi.org/10.1016/j.earscirev.2004.05.001.

Coulon, C., Maluski, H., Bollinger, C., and Wang, S., 1986, Mesozoic and Cenozoic volcanic rocks from central and southern Tibet: ^{39}Ar-^{40}Ar dating, petrological characteristics and geodynamical significance: Earth and Planetary Science Letters, v. 79, p. 281–302, https://doi.org/10.1016/0012-821X(86)90186-X.

Davies, J.H., and von Blanckenburg, F., 1995, Slab breakoff: A model of lithosphere detachment and its test in the magmatism and deformation of collisional orogens: Earth and Planetary Science Letters, v. 129, p. 85–102, https://doi.org/10.1016/0012-821X(94)00237-S.

Defant, M.J., and Drummond, M.S., 1990, Derivation of some modern arc magmas by melting of young subducted lithosphere: Nature, v. 347, p. 662–665, https://doi.org/10.1038/347662a0.

Dewey, J.F., Shackleton, R.M., Chang, C., and Sun, Y., 1988, The tectonic evolution of the Tibetan Plateau: Philosophical Transactions of the Royal Society of London Series A, v. 327, p. 379–413, https://doi.org/10.1098/rsta.1988.0135.

Didier, J., and Barbarin, B., 1991, The different types of enclaves in granites, *in* Didier, J., and Barbarin, B., eds., Enclaves and granite petrology: Developments in Petrology, v. 13, p. 19–24.

Ding, L., Kapp, P., Zhong, D., and Deng, W., 2003, Cenozoic volcanism in Tibet: Evidence for a transition from oceanic to continental subduction: Journal of Petrology, v. 44, p. 1833–1865, https://doi.org/10.1093/petrology/egg061.

Dong, H., Gou, G.N., Qi, Y., Duan, K., Zhang, Z.P., Wu, Y., Jiao, S.W., Hao, L.L., Chen, F.K., and Wang, Q., 2016, Late Early Cretaceous crustal growth in northern Lhasa Block: Evidence from ca. 106 Ma intrusive rocks in the Yaduo area, Gerze County: Geotecto et Metallo, v. 40, p. 1226–1238 (in Chinese with English abstract).

Fielding, E.J., 1996, Tibet uplift and erosion: Tectonophysics, v. 260, p. 55–84, https://doi.org/10.1016/0040-1951(96)00076-5.

Gao, S., Rudnick, R.L., Yuan, H.L., Liu, X.M., Liu, Y.S., Xu, W.L., Lin, W.L., Ayers, J., Wang, X.C., and Wang, Q.H., 2004, Recycling lower continental crust in the North China craton: Nature, v. 432, p. 892–897, https://doi.org/10.1038/nature03162.

Goto, A., and Tatsumi, Y., 1994, Quantitative analysis of rock samples by an X-ray fluorescence spectrometer (I): The Rigaku Journal, v. 11, p. 40–59.

Guo, F., Nakamuru, E., Fan, W.M., Kobayoshi, K., and Li, C.W., 2007, Generation of Palaeocene adakitic andesites by magma mixing; Yanji Area, NE China: Journal of Petrology, v. 48, p. 661–692, https://doi.org/10.1093/petrology/egl077.

Hastie, A.R., Kerr, A.C., Pearce, J.A., and Mitchell, S.F., 2007, Classification of altered volcanic island arc rocks using immobile trace elements: development of the Th–Co discrimination diagram: Journal of Petrology, v. 48, p. 2341–2357, https://doi.org/10.1093/petrology/egm062.

Hetzel, R., Dunkl, I., Haider, V., Strobl, M., von Eynatten, H., Ding, L., and Frei D., 2011, Peneplain formation in southern Tibet predates the India-Asia collision and plateau uplift: Geology, v. 39, p. 983–986, https://doi.org/10.1130/G32069.1.

Holden, P., Halliday, A.N., and Stephens, W.E., 1987, Neodymium and strontium isotope content of microdiorite enclaves points to mantle input to granitoid production: Nature, v. 330, p. 53–56, https://doi.org/10.1038/330053a0.

Hou, Z., Gao, Y., Qu, X., Rui, Z., and Mo, X., 2004, Origin of adakitic intrusives generated during mid-Miocene east-west extension in southern Tibet: Earth and Planetary Science Letters, v. 220, p. 139–155, doi:10.1016/S0012-821X(04)00007-X.

Hu, F.Y., Ducea, M.N., Liu, S.W., and Chapman, J.B., 2017, Quantifying crustal thickness in continental collisional belts: Global perspective and a geologic application: Scientific Reports, v. 7, p. 7058, https://doi.org/10.1038/s41598-017-07849-7.

Janoušek, V., Braithwaite, C.J.R., Bowes, D.R., and Gerdes, A., 2004, Magma mixing in the genesis of Hercynian calc-alkaline granitoids: An integrated petrographic and geochemical study of the Sazava intrusion, Central Bohemian Pluton, Czech Republic: Lithos, v. 78, p. 67–99, https://doi.org/10.1016/j .lithos.2004.04.046.

Ji, W.Q., Wu, F.Y., Chung, S.L., Li, J.X., and Liu, C.Z., 2009, Zircon U-Pb chronology and Hf isotopic constraints on the petrogenesis of Gangdese batholiths, southern Tibet: Chemical Geology, v. 262, p. 229–245, https://doi.org/10.1016/j.chemgeo.2009.01.020.

Jiang, Y.S., Zhou, Y.Y., and Li, J.B. 2002, 1:250,000 geological map of Coqen area: Press of China University of Geoscience (in Chinese).

Kang, Z.Q., Xu, J.F., Dong, Y.H., and Wang, B.D., 2008, Cretaceous volcanic rocks of Zenong Group in north-middle Lhasa block: products of southward subducting of the Slainajap Ocean?: Acta Petrolei Sinica, v. 24, p. 303–314 (in Chinese with English abstract).

Kang, Z.Q., Xu, J.F., Wang, B.D., Dong, Y.H., Wang, S.Q., and Chen, J.L., 2009, Geochemistry of Cretaceous volcanic rocks of Duoni Formation in northern Lhasa block: discussion of tectonic setting: Earth Science-Journal of China University of Geosciences, v. 34, p. 89–104 (in Chinese with English abstract).

Kang, Z.Q., Xu, J.F., Wang, B.D., and Chen, J.L., 2010, Qushenla Formation volcanic rocks in north Lhasa block: Products of Bangong Co-Nujiang Tethys southward subduction: Acta Petrolei Sinica, v. 26, p. 3106–3116 (in Chinese with English abstract).

Kapp, P., Yin, A., Harrison, T.M., and Ding, L., 2005, Cretaceous-Tertiary shortening, basin development, and volcanism in central Tibet: Geological Society of America Bulletin, v. 117, p. 865–878, https://doi.org/10.1130 /B25595.1.

Kapp, P., DeCelles, P.G., Gehrels, G.E., Heizler, M., and Ding, L., 2007, Geological records of the Lhasa-Qiangtang and Indo-Asian collisions in the Nima area of central Tibet: Geological Society of America Bulletin, v. 119, p. 917–933, https://doi.org/10.1130/B26033.1.

Kohn, M.J., and Parkinson, C.D., 2002, Petrologic case for Eocene slab breakoff during the Indo-Asian collision: Geology, v. 30, p. 591–594, https://doi.org/10.1130/0091-7613(2002)030<0591:PCFESB>2.0.CO;2.

Koschek, G., 1993, Origin and significance of the SEM cathodoluminescence from zircon: Journal of Microscopy, v. 171, p. 223–232, https://doi.org/10.1111/j.1365-2818.1993.tb03379.x.

Lai, W., Hu, X.M., Zhu, D.C., An, W., and Ma, A.L., 2017, Discovery of the early Jurassic Gajia mélange in the Bangong-Nujiang suture zone: Southward subduction of the Bangong-Nujiang Ocean: International Journal of Earth Sciences, v. 106, p. 1277–1288, https://doi.org/10.1007/s00531-016-1405-1.

Lee, C.T.A., Thurner, S., Paterson, S., and Cao, W., 2015, The rise and fall of continental arcs: Interplays between magmatism, uplift, weathering, and climate: Earth and Planetary Science Letters, v. 425, p. 105–119, https://doi.org/10.1016/j.epsl.2015.05.045.

Lei, M., Chen, J.L., Xu, J.F., and Zeng, Y.C., 2015, Geochemistry of Early Late Cretaceous Gaerqiong high-Mg# diorite porphyry in mid-northern Lhasa terrane: Partial melting of delaminated lower continental crust: Geological Bulletin of China, v. 34, p. 337–346 (in Chinese with English abstract).

Li, D.W., 2008, Three-stage tectonic evolution and metallogenic evolution in the Qinghai-Tibet Plateau and its adjacent area: Earth Science-Journal of China University of Geosciences, v. 33, p. 723–742 (in Chinese with English abstract).

Li, G.M., Qin, K.Z., Li, J.X., Evans, N.J., Zhao, J.X., Cao, M.J., and Zhang, X.N., 2017, Cretaceous magmatism and metallogeny in the Bangong–Nujiang metallogenic belt, central Tibet: evidence from petrogeochemistry, zircon U–Pb ages, and Hf–O isotopic compositions: Gondwana Research, v. 41, p. 110–127, https://doi.org/10.1016/j.gr.2015.09.006.

Li, H.L., 2014, Signs and Time of Ocean- Continent Transform of the Western Part of Bangong–Nujiang Suture Zone [Ph.D. dissertation]: China University of Geosciences, Wuhan (in Chinese with English abstract).

Li, X.H., Li, Z.X., Wingate, M.T.D., Chung, S.L., Liu, Y., Lin, G.C., and Li, W.X., 2006, Geochemistry of the 755 Ma Mundine Well dyke swarm, northwestern Australia: part of a Neoproterozoic mantle superplume beneath Rodinia: Precambrian Research, v. 146, p. 1–15, https://doi.org/10.1016/j.precamres.2005.12.007.

Li, X.H., Long, W.G., Li, Q.L., Liu, Y., Zheng, Y.F., Yang, Y.H., Chamberlain, K.R., Wan, D.F., Guo, C.H., and Wang, X.C., 2010, Penglai zircon megacrysts: a potential new working reference material for microbeam determination of Hf–O isotopes and U–Pb age: Geostandards and Geoanalytical Research, v. 34, p. 117–134, https://doi.org/10.1111/j.1751-908X.2010.00036.x.

Li, Y.L., He, J., Wang, C.S., Santosh, M., Dai, J.G., Zhang, Y.X., Wei, Y.S., and Wang, J.G., 2013, Late Cretaceous K-rich magmatism in central Tibet: evidence for early elevation of the Tibetan plateau?: Lithos, v. 160, p. 1–13, https://doi.org/10.1016/j.lithos.2012.11.019.

Liu, D., Zhao, Z.D., Zhu, D.C., Niu, Y.L., and Harrison, T.M., 2014, Zircon xenocrysts in Tibetan ultrapotassic magmas: Imaging the deep crust through time: Geology, v. 42, p. 43–46, https://doi.org/10.1130/G34902.1.

Liu, H., Wang, B.D., Chen, L., Li, X.B., and Wang, L.Q., 2015, Zircon U-Pb geochronology, geochemistry and its tectonic significance of the Rutog granitic batholith in the Northwest Lhasa Terrane: Geotectonica et Metallogenia, v. 39, p. 1141–1155 (in Chinese with English abstract).

Ludwig, K.R., 2003, User's manual for Isoplot, v. 3.00, a geochronological toolkit for Microsoft Excel: Berkeley Geochronological Center Special Publication, v. 4, p. 47–93.

Lustrino, M., 2005, How the delamination and detachment of lower crust can influence basaltic magmatism: Earth-Science Reviews, v. 72, p. 21–38, https://doi.org/10.1016/j.earscirev.2005.03.004.

Lv, L.N., 2012, Metallogenic model of rich iron and copper(gold) deposit in western part of Bangong Co-Nujiang metallogenic belt, Tibet [master's degree dissertation: Chinese Academy of Geological Sciences, Beijing (in Chinese with English abstract).

Ma, G.L., and Yue, Y.H., 2010, Cretaceous volcanic rocks in northern Lhasa Block: constraints on the tectonic evolution of the Gangdese Arc: Acta Petrolei et Mineralogica, v. 29, p. 525–538 (in Chinese with English abstract).

Ma, L., Wang, Q., Wyman, D.A., Jiang, Z.Q., Wu, F.Y., Li, X.H., Yang, J.H., Gou, G.N., and Guo, H.F., 2015, Late Cretaceous back-arc extension and arc system evolution in the Gangdese area, southern Tibet: Geochronological, petrological, and Sr-Nd-Hf-O isotopic evidence from Dagze diabases: Journal of Geophysical Research. Solid Earth, v. 120, p. 6159–6181, https://doi.org/10.1002/2015JB011966.

Macera, P.M., Gasperini, D., Ranalli, G., and Mahatsent, R., 2008, Slab detachment and mantle plume upwelling in subduction zones: an example from the Italian South-Eastern Alps: Journal of Geodynamics, v. 45, p. 32–48, https://doi.org/10.1016/j.jog.2007.03.004.

Macpherson, C.G., Dreher, S.T., and Thirlwall, M.F., 2006, Adakites without slab melting: high pressure differentiation of island arc magma, Mindanao, the Philippines: Earth and Planetary Science Letters, v. 243, p. 581–593, https://doi.org/10.1016/j.epsl.2005.12.034.

Mahéo, G., Guillot, S., Blichert-Toft, J., Rolland, Y., and Pecher, A., 2002, A slab breakoff model for the Neogene thermal evolution of South Karakorum and South Tibet: Earth and Planetary Science Letters, v. 195, p. 45–58, https://doi.org/10.1016/S0012-821X(01)00578-7.

Maniar, P.D., and Piccoli, P.M., 1989, Tectonic discrimination of granitoids: Geological Society of America Bulletin, v. 101, p. 635–643, https://doi.org/10.1130/0016-7606(1989)101<0635:TDOG>2.3.CO;2.

Martin, H., Smithies, R.H., Rapp, R., Moyen, J.F., and Champion, D.C., 2005, An overview of adakite, tonalite–trondhjemite–granodiorite (TTG), and sanukitoid: Relationships and some implications for crustal evolution: Lithos, v. 79, p. 1–24, https://doi.org/10.1016/j.lithos.2004.04.048.

Mo, X.X., Hou, Z.Q., Niu, Y.L., Dong, G.C., Qu, X.M., Zhao, Z.D., and Yang, Z.M., 2007, Mantle contributions to crustal thickening during continental collision: Evidence from Cenozoic igneous rocks in southern Tibet: Lithos, v. 96, p. 225–242, https://doi.org/10.1016/j.lithos.2006.10.005.

Mo, X.X., Niu, Y.L., Dong, G.C., Zhao, Z.D., Hou, Z.Q., Zhou, S., and Ke, S., 2008, Contribution of syncollisional felsic magmatism to continental crust growth: a case study of the Paleogene Linzizong volcanic succession in southern Tibet: Chemical Geology, v. 250, p. 49–67, https://doi.org/10.1016/j.chemgeo.2008.02.003.

Murphy, M.A., Yin, A., Harrison, T.M., Dürr, S.B., Chen, Z., Ryerson, F.J., Kidd, W.S.F., Wang, X., and Zhou, X., 1997, Did the Indo-Asian collision alone create the Tibetan plateau: Geology, v. 25, p. 719–722, https://doi.org/10.1130/0091-7613(1997)025<0719:DTIACA>2.3.CO;2.

Pan, G.T., and Ding, J., 2004, Geological map (1:1,500,000) of Qinghai-Xizang (Tibetan) Plateau and adjacent areas: Chengdu, Chengdu Cartographic Publishing House.

Pan, G.T., Mo, X.X., Hou, Z.Q., Zhu, D.C., Wang, L.Q., Li, G.M., Zhao, Z.D., Geng, Q.R., and Liao, Z.L., 2006, Spatial-temporal framework of the Gangdese Orogenic Belt and its evolution: Acta Petrolei Sinica, v. 22, p. 521–533 (in Chinese with English abstract).

Perkins, J.P., Ward, K.M., De Silva, S.L., Zandt, G., Beck, S.L., and Finnegan, N.J., 2016, Surface uplift in the Central Andes driven by growth of the Altiplano Puna magma body: Nature Communications, v. 7, p. 13185, https://doi.org/10.1038/ncomms13185.

Profeta, L., Ducea, M.N., Chapman, J.B., Paterson, S.R., Gonzales, S.M., Kirsch, M., Petrescu, L., and DeCelles, P.G., 2015, Quantifying crustal thickness over time in magmatic arcs: Scientific Reports, v. 5, 17786, https://doi.org/10.1038/srep17786.

Qiu, R.Z., Zhou, S., Li, T.D., Deng, J.F., Xiao, Q.H., Wu, Z.X., and Cai, Z.Y., 2007, The tectonic setting of ophiolites in the western Qinghai-Tibet Plateau, China: Journal of Asian Earth Sciences, v. 29, p. 215–228, https://doi.org/10.1016/j.jseaes.2006.06.007.

Qu, X.M., Xin, H.B., Xu, W.Y., Yang, Z.S., and Li, Z.Q., 2006, Discovery and significance of copper-bearing bimodal rocks series in Coqin area of Tibet: Acta Petrolei Sinica, v. 22, p. 707–716 (in Chinese with English abstract).

Rapp, R.P., and Watson, E.B., 1995, Dehydration melting of metabasalt at 8–32-kbar: Implications for continental growth and crust–mantle recycling: Journal of Petrology, v. 36, p. 891–931, https://doi.org/10.1093/petrology/36.4.891.

Rapp, R.P., Shimizu, N., Norman, M.D., and Applegate, G.S., 1999, Reaction between slab-derived melts and peridotite in the mantle wedge: Experimental constraints at 3.8 GPa: Chemical Geology, v. 160, p. 335–356, https://doi.org/10.1016/S0009-2541(99)00106-0.

Rohrmann, A., Kapp, P., Carrapa, B., Reiners, P.W., Guynn, J., Ding, L., and Heizler, M., 2012, Thermochronologic evidence for plateau formation in central Tibet by 45 Ma: Geology, v. 40, p. 187–190, https://doi.org/10.1130/G32530.1.

Rollinson, H.R., 1993, Using Geochemical Data: Evaluation, Presentation, Interpretation: , London, Longman Scientific & Technical, p. 108.

Rudnick, R.L., 1995, Making continental crust: Nature, v. 378, p. 571–578, https://doi.org/10.1038/378571a0.

Rudnick, R.L., and Gao, S., 2003, Composition of the continental crust, *in* Holland, H.D., and Turekian, K.K., The Crust: Amsterdam, Elsevier, Treatise on Geochemistry, v. 3, p. 1–64, https://doi.org/10.1016/B0-08-043751-6/03016-4.

Schonenberger, J., Marks, M., Wagner, T., and Markl, G., 2006, Fluid–rock interaction in autoliths of agpaitic nepheline syenites in the Ilimaussaq intrusion, South Greenland: Lithos, v. 91, p. 331–351, https://doi.org/10.1016/j.lithos.2006.03.024.

Shimoda, G., Tatsumi, Y., Nohda, S., Ishizaka, K., and Jahn, B., 1998, Setouchi high-Mg andesites revisited: geochemical evidence for melting of subducting sediments: Earth and Planetary Science Letters, v. 160, p. 479–492, https://doi.org/10.1016/S0012-821X(98)00105-8.

Shirey, S.B., and Hanson, G.N., 1984, Mantle-derived Archaean monozodiorites and trachyandesites: Nature, v. 310, p. 222–224, https://doi.org/10.1038/310222a0.

Soesoo, A., 2000, Fractional crystallization of mantle derived melts as a mechanism for some I-type granite petrogenesis: an example from Lachlan Fold Belt: Journal of the Geological Society, v. 157, p. 135–149, https://doi.org/10.1144/jgs.157.1.135.

Sparks, R.S.J., and Marshall, L.A., 1986, Thermal and mechanical constraints on mixing between mafic and silicic magmas: Journal of Volcanology and Geothermal Research, v. 29, p. 99–124, https://doi.org/10.1016/0377-0273(86)90041-7.

Streck, M.J., Leeman, W.P., and Chesley, J., 2007, High magnesian andesite from Mount Shasta: A product of magma mixing and contamination, not a primitive mantle melt: Geology, v. 35, p. 351–354, https://doi.org/10.1130/G23286A.1.

Sui, Q.L., Wang, Q., Zhu, D.C., Zhao, Z.D., Chen, Y., Santosh, M., Hu, Z.C., Yuan, H.L., and Mo, X.X., 2013, Compositional diversity of ca. 110 Ma magmatism in the northern Lhasa Terrane, Tibet: Implications for the magmatic origin and crustal growth in a continent–continent collision zone: Lithos, v. 168, p. 144–159, https://doi.org/10.1016/j.lithos.2013.01.012.

Sun, S., and McDonough, W.F., 1989, Chemical and isotopic systematics of oceanic basalts: Implications for mantle composition and processes, in Saunders, A.D., and Norry, M.J., eds., Magmatism in the Ocean Basins: Geological Society, London, Special Publication 42, p. 313–345, https://doi.org/10.1144/GSL.SP.1989.042.01.19.

Sun, G.Y., Hu, X.M., Sinclair, H.D., Marcelle, B.D., and Wang, J.G., 2015a, Late Cretaceous evolution of the Coqen basin (Lhasa terrane) and implications for early topographic growth on the Tibetan Plateau: Geological Society of America Bulletin, v. 127, p. 1001–1020, 10.1130/B31137.1.

Sun, G.Y., Hu, X.M., Zhu, D.C., Hong, W.T., Wang, J.G., and Wang, Q., 2015b, Thickened juvenile lower crust-derived ~90 Ma adakitic rocks in the central Lhasa terrane, Tibet: Lithos, v. 224, p. 225–239, https://doi.org/10.1016/j.lithos.2015.03.010.

Tapponnier, P., Xu, Z., Rogers, F., Meyer, B., Arnaud, N., Wittlinger, G., and Yang, J., 2001, Oblique stepwise rise and growth of the Tibet Plateau: Science, v. 294, p. 1671–1677, https://doi.org/10.1126/science.105978.

Troll, V.R., and Schmincke, H.U., 2002, Magma mixing and crustal recycling recorded in ternary feldspar from compositionally zoned peralkaline ignimbrite "A," Gran Canaria, Canary Islands: Journal of Petrology, v. 43, p. 243–270, https://doi.org/10.1093/petrology/43.2.243.

Turner, S., Hawkesworth, C., Liu, J.Q., Rogers, N., Kelley, S., and van Calsteren, P., 1993, Timing of Tibetan uplift constrained by analysis of volcanic rocks: Nature, v. 364, p. 50–54, https://doi.org/10.1038/364050a0.

Turner, S., Arnaud, N., Liu, J., Rogers, N., Hawkesworth, C., Harris, N., and Kelley, S., 1996, Post-collision, shoshonitic volcanism on the Tibetan Plateau: Implications for convective thinning of the lithosphere and the source of ocean island basalts: Journal of Petrology, v. 37, p. 45–71, https://doi.org/10.1093/petrology/37.1.45.

van Hunen, J., and Allen, M.B., 2011, Continental collision and slab break-off: A comparison of 3-D numerical models with observations: Earth and Planetary Science Letters, v. 302, p. 27–37, https://doi.org/10.1016/j.epsl.2010.11.035.

Vernon, R.H., and Williams, P.F., 1988, Distinction between intrusive and extrusive or sedimentary parentage of felsic gneisses: examples from the Broken Hill Block, NSW: Australian Journal of Earth Sciences, v. 35, p. 379–388, https://doi.org/10.1080/08120098808729455.

Volkmer, J.E., Kapp, P., Guynn, J.H., and Lai, Q., 2007, Cretaceous-Tertiary structural evolution of the north central Lhasa terrane, Tibet: Tectonics, v. 26, TC6007, https://doi.org/10.1029/2005TC001832.

Wang, B.D., Wang, L.Q., Chung, S.L., Chen, J.L., Yin, F.G., Liu, H., Li, X.B., and Chen, L.K., 2016a, Evolution of the Bangong-Nujiang Tethyan ocean: Insights from the geochronology and geochemistry of mafic rocks within ophiolites: Lithos, v. 245, p. 18–33, https://doi.org/10.1016/j.lithos.2015.07.016.

Wang, C., Zhao, X., Liu, Z., Lippert, P.C., Graham, S.A., Coe, R.S., Yi, H., Zhu, L., Liu, S., and Li, Y., 2008, Constraints on the early uplift history of the Tibetan Plateau: Proceedings of the National Academy of Sciences of the United States of America, v. 105, p. 4987–4992, https://doi.org/10.1073 /pnas.0703595105.

Wang, J.G., Hu, X.M., Garzanti, E., Ji, W.Q., Liu, Z.C., Liu, X.C., and Wu, F.Y., 2017, Early cretaceous topographic growth of the Lhasaplano, Tibetan plateau: Constraints from the Damxung conglomerate: Journal of Geophysical Research. Solid Earth, v. 122, p. 5748–5765, https://doi.org/10.1002/2017JB014278.

Wang, Q., Xu, J.F., Jian, P., Bao, Z.W., Zhao, Z.H., Li, C.F., Xiong, X.L., and Ma, J.L., 2006, Petrogenesis of adakitic porphyries in an extensional tectonic setting, Dexing, South China: Implications for the genesis of porphyry copper mineralization: Journal of Petrology, v. 47, p. 119–144, https://doi.org/10.1093/petrology/egi070.

Wang, Q., Zhu, D.C., Zhao, Z.D., Liu, S.A., Chung, S.L., Li, S.M., Liu, D., Dai, J.G., Wang, L.Q., and Mo, X.X., 2014, Origin of the ca. 90 Ma magnesia-rich volcanic rocks in SW Nyima, central Tibet: Products of lithospheric delamination beneath the Lhasa-Qiangtang collision zone: Lithos, v. 198–199, p. 24–37, https://doi.org/10.1016 /j. lithos.2014. 03. 019.

Wang, X.C., Wilde, S.A., Xu, B., and Pang, C.J., 2016b, Origin of arc-like continental basalts: implications for deep-Earth fluid cycling and tectonic discrimination: Lithos, v. 261, p. 5–45, https://doi.org/10.1016/j.lithos.2015.12.014.

Watson, E.B., and Harrison, T.M., 1983, Zircon saturation revisited: Temperature and composition effects in a variety of crustal magma types: Earth and Planetary Science Letters, v. 64, p. 295–304, https://doi.org/10.1016/0012-821X(83)90211-X.

White, A.J.R., and Chappell, B.W., 1977, Ultrametamorphism and granitoid genesis: Tectonophysics, v. 43, p. 7–22, https://doi.org/10.1016/0040-1951(77)90003-8.

Wilson, B.M., 1989, Igneous Petrogenesis: A Global Tectonic Approach: Dordrecht, Springer, 466 p, https://doi.org/10.1007/978-1-4020-6788-4.

Wu, F.Y., Ji, W.Q., Liu, C.Z., and Chung, S.L., 2010, Detrital zircon U-Pb and Hf isotopic data from the Xigaze forearc basin: Constraints on Transhimalayan magmatic evolution in southern Tibet: Chemical Geology, v. 271, p. 13–25, https://doi.org/10.1016/j.chemgeo.2009.12.007.

Xin, H.B., Qu, X.M., Ren, L.K., and Zhang, L.Y., 2007, The material source and genesis of copper-bearing bimodal rocks series in Coqin County, Western Tibet: Acta Geologica Sinica, v. 81, p. 939–935 (in Chinese with English abstract).

Xu, J.F., Shinjo, R., Defant, M.J., Wang, Q., and Rapp, R.P., 2002, Origin of Mesozoic adakitic intrusive rocks in the Ningzhen area of east China: Partial melting of delaminated lower continental crust?: Geology, v. 30, p. 1111–1114, https://doi.org/10.1130/0091-7613(2002)030<1111:OOMAIR>2.0.CO;2.

Xu, R.H., Schärer, U., and Allègre, C.J., 1985, Magmatism and metamorphism in the Lhasa block (Tibet): A geochronological study: The Journal of Geology, v. 93, p. 41–57, https://doi.org/10.1086/628918.

Yang, J.H., Wu, F.Y., Chung, S.L., Wilde, S.A., and Chu, M.F., 2006, A hybrid origin for the Qianshan A-type granite, northeast China: Geochemical and Sr-Nd-Hf isotopic evidence: Lithos, v. 89, p. 89–106, https://doi.org/10.1016/j.lithos.2005.10.002.

Yao, X.F., Tang, J.X., Li, Z.J., Deng, S.L., Ding, S.H., Zheng, H., and Zhang, Z., 2012, Magma origin of two plutons from Gaerqiong copper-gold deposit and its geological significance, western Bangonghu-Nujiang metallogenic belt, Tibet implication from Hf isotope characteristics: Journal of Jilin University, v. 42, p. 188–197 (in Chinese with English abstract).

Yi, J.K., Wang, Q., Zhu, D.C., Li, S.M., Liu, S.A., Wang, R., Zhang, L.L., and Zhao, Z.D., 2018, Westward-younging high-Mg adakitic magmatism in Central Tibet: Record of a westward-Migrating lithospheric foundering beneath the Lhasa-Qiangtang collision zone during the late Cretaceous: Lithos, v. 316–317, p. 92–103, https://doi.org/10.1016/j.lithos.2018.07.001.

Yin, A., and Harrison, T.M., 2000, Geologic evolution of the Himalayan-Tibetan orogen: Annual Review of Earth and Planetary Sciences, v. 28, p. 211–280, https://doi.org/10.1146/annurev.earth.28.1.211.

Yu, H.X., Chen, J.L., Xu, J.F., Wang, B.D., Wu, J.B., and Liang, Y.H., 2011, Geochemistry and origin of Late Cretaceous (~90 Ma) mineral porphyry of Balazha in mid-northern Lhasa terrane, Tibet: Acta Petrolei Sinica, v. 27, p. 2011–2022 (in Chinese with English abstract).

Yuan, H.L., Gao, S., Dai, M.N., Zong, C.L., Gunther, D., Fontaine, G.H., Liu, X.M., and Diwu, C.R., 2008, Simultaneous determinations of U-Pb age, Hf isotopes and trace element compositions of zircon by excimer laser-ablation quadrupole and multiple-collector ICP-MS: Chemical Geology, v. 247, p. 100–118, https://doi.org/10.1016/j.chemgeo.2007.10.003.

Zhang, H.F., Parrish, R., Zhang, L., Xu, W.C., Yuan, H.L., Gao, S., and Crowley, Q.G., 2007, A-type

granite and adakitic magmatism association in Songpan-Garze fold belt, eastern Tibetan Plateau: Implication for lithospheric delamination: Lithos, v. 97, p. 323–335, https://doi.org/10.1016/j.lithos.2007.01.002.

Zhang, K.J., Zhang, Y., Tang, X., and Xia, B., 2012, Late Mesozoic tectonic evolution and growth of the Tibetan plateau prior to the Indo-Asian collision: Earth Science Reviews, v. 114, p. 236–249, https://doi.org/10.1016/j.earscirev.2012.06.001.

Zhang, S., Shi, H.F., Hao, H.J., Li, D.W., Lin, Y., and Feng, M.X., 2014, Geochronology, geochemistry and tectonic significance of Early Late Cretaceous adakites in Bangong Lake, Tibet: Earth Science-Journal of China University of Geosciences, v. 39, p. 509–524 (in Chinese with English abstract).

Zhang, X.Q., 2012, Geochronology and Geochemistry of the Maiga batholith in Coqen, Tibet-constraints on the petrogenesis of Early Cretaceous granitoids in central Lhasa terrane a [master's degree dissertation]: China University of Geosciences, Beijing (in Chinese with English abstract).

Zhang, Y.Y., Sun, M., Yuan, C., Xu, Y.G., Long, X.P., Tomurhun, D., Wang, C.Y., and He, B., 2015, Magma mixing origin for high Ba–Sr granitic pluton in the Bayankhongor area, central Mongolia: Response to slab roll-back: Journal of Asian Earth Sciences, v. 113, p. 353–368, https://doi.org/10.1016/j.jseaes.2014.11.029.

Zhao, T.P., Zhou, M.F., Zhao, J.H., Zhang, K.J., and Chen, W., 2008, Geochronology and geochemistry of the ca. 80 Ma Rutog granitic pluton, northwestern Tibet: implications for the tectonic evolution of the Lhasa Terrane: Geological Magazine, v. 145, p. 845–857, https://doi.org/10.1017/S0016756808005025.

Zhou, C.Y., Zhu, D.C., Zhao, Z.D., Xu, J.F., Wang, L.Q., Chen, H.H., Xie, L.W., Dong, G.C., and Zhou, S., 2008, Petrogenesis of Daxiong pluton in western Gangdese, Tibet: zircon U-Pb dating and Hf isotopic constraints: Acta Petrolei Sinica, v. 24, p. 348–358 (in Chinese with English abstract).

Zhu, D.C., Mo, X.X., Niu, Y.L., Zhao, Z.D., Wang, L.Q., Liu, Y.S., and Wu, F.Y., 2009, Geochemical investigation of Early Cretaceous igneous rocks along an east-west traverse throughout the central Lhasa Terrane, Tibet: Chemical Geology, v. 268, p. 298–312, https://doi.org/10.1016/j.chemgeo.2009.09.008.

Zhu, D.C., Zhao, Z.D., Niu, Y.L., Mo, X.X., Chung, S.L., Hou, Z.Q., Wang, L.Q., and Wu, F.Y., 2011, The Lhasa Terrane: Record of a microcontinent and its histories of drift and growth: Earth and Planetary Science Letters, v. 301, p. 241–255, https://doi.org/10.1016/j.epsl.2010.11.005.

Zhu, D.C., Zhao, Z.D., Niu, Y.L., Dilek, Y., Hou, Z.Q., and Mo, X.X., 2013, The origin and pre-Cenozoic evolution of the Tibetan Plateau: Gondwana Research, v. 23, p. 1429–1454, https://doi.org/10.1016/j.gr.2012.02.002.

Science Editor: Bradley S. Singer
Associate Editor: Haibo Zou

Manuscript Received 25 August 2017
Revised Manuscript Received 8 December 2018
Manuscript Accepted 17 February 2019

Printed in the USA